NASA Technical Memorandum 104056

Time Domain Reflectometry in Time Variant Plasmas

Michael J. Scherner

September 1992

National Aeronautics and Space Administration

Langley Research Center
Hampton, Virginia 23665-5225

TABLE OF CONTENTS

SECTION 1
INTRODUCTION

Time domain reflectometry measurements in plasmas are of great interest. This is particularly true in studying the high density plasma layer which forms around a spacecraft as it reenters the Earth's atmosphere. It is well established that heat transfer rates for spacecraft in reentry can be greatly influenced by flowfield ionization levels. Knowledge of the ionization level is, therefore, important during reentry as a function of body station, especially in the forebody region. Current analytical models are unverified and incumbered with unproven simplifying assumptions and, as a result, fall short of providing dependable electron density predictions.

The Microwave Reflectometer Ionization Sensor (MRIS) Experiment[1] will make use of the microwave reflection properties of ionized gases to determine levels of electron density in the forebody shock layer of a reentry vehicle and to measure the distance from the vehicle at which these electron densities occur. Specifically, the experiment will locate the onset and presence of critical electron densities corresponding to selected carrier frequencies by measuring the amplitude and phase of the reflected signal. The critical electron density is the density at which a rapid increase in reflection coefficient occurs. The distance to the critical density point will be obtained through time domain reflectometry using 64 equally spaced transmitted frequencies, occupying a total bandwidth of 2 GHz. At the receiver, 64 frequency responses are collected and an inverse

[1] NASA experiment originally proposed for 1996

fast Fourier transform then provides a time domain impulse response for the plasma. The propagation delays of the signals reflected from the ionized flow field will be measured to determine the stand-off distances to the location of the critical electron densities detected. The stand-off distance information for the vehicle will be compared to the data predicted from the computational fluid dynamics models for the spacecraft's trajectory. Such a procedure should work well so long as the properties of the plasma layer are constant over the time required for the 64 measurements. Since the positions of the critical electron densities will fluctuate during measurement periods, it is desirable to study the effects of any such fluctuations on the time domain reflectometry response. The purpose of this paper is to study the effects of time dependent-fluctuations on time domain reflectometry for a one-dimensional plasma sheath.

The study of plane waves incident on stable plasma layers has been investigated by many authors [1-5]. Their work has been focused on solving the differential equations which describe the electromagnetic behavior of fields within these fixed layers. This paper delves into the electromagnetic behavior of fields within a time-variant plasma layer. Solutions for continuous inhomogeneous layers require, in general, numerical techniques. In this paper the plasma is represented by a one-dimensional dielectric constant which is allowed to vary in the direction of propagation. Practical solutions have been obtained using numerical methods for solving the Helmholtz wave equation describing propagation through the plasma layer. Sequences of density profiles have been generated to emulate the time-dependent behavior of moving density fluctuations. The plasma has been studied for a range of constituent transmitted frequencies (64 stepped frequencies), consistent

with the MRIS experiment, and the resulting responses have been used to synthesize effective time domain responses.

Broadly speaking, this paper is divided into four parts. Section 2 deals with the models used for a given plasma layer which can be represented by a dielectric medium with a dielectric constant which can have a negative imaginary part representing losses as explained in reference 6. Section 3 concentrates on reflection coefficients for different plasma models. To simulate the time domain reflectometry response of a fixed one-dimensional cold plasma sheath, solutions for the electric field of a normally incident plane wave in a specified electron density are used. Illustrative cases with simplified profiles with exact solutions are presented for the reader in this section. Section 4 looks at simulating the time domain response of the plasma by mathematically transforming reflection coefficient measurements made in the frequency domain. From the responses, propagation delays of the signals reflected were measured to determine the distances to the location of the critical electron densities. Section 5 investigates electron density fluctuations and their effect on time domain responses. For the sake of clarity, many of the problems treated are greatly simplified. For instance in Section 3, a homogeneous layer and a linear layer are examined as illustrative aids for understanding the solutions for a inhomogeneous plasma layer. The appendix reviews the time domain theory used in this paper. A computer program was developed to solve inhomogeneous plasma layer problems. For propagation studies, a time harmonic wave traveling in the positive z-direction with an $e^{-i\omega t}$ time convention is assumed throughout the paper. Normal incidence was chosen to simplify problems and to help focus on the intent of the paper. Issues and considerations regarding the MRIS distance-measuring scheme are discussed

in the conclusion.

SECTION 2
ELECTRON PLASMA MODEL

2.1 Wave Propagation

In the solution of any electromagnetic problem, Maxwell's equations must be satisfied. As shown in reference 7, these equations can be used to obtain a differential equation describing wave propagation through an arbitrary medium. This differential equation known as the one-dimensional Helmholtz wave equation is written as

$$\frac{\partial^2 E(z)}{\partial z^2} + \omega^2 \mu \varepsilon(z) E(z) = 0 \qquad (2.1)$$

where E is the electric field intensity, ω is the radian frequency, μ is the permeability of the medium, and ε is the dielectric constant of the medium which is shown as a function of z, the axis along which the electromagnetic fields propagate. For the case where ε does not depend on z (purely homogeneous dielectric), a time-harmonic wave moving in the positive z-direction, with an $e^{-i\omega t}$ time convention, results in a solution written as

$$E(z) = E_1 e^{ikz} + E_2 e^{-ikz} \quad , \qquad (2.2)$$

where E_1 and E_2 are undetermined constants independent of z and k, the wavenumber, is

$$k = \omega \sqrt{\mu \varepsilon_r \varepsilon_o} \quad , \qquad (2.3)$$

ε_r is the relative dielectric constant of the medium and ε_o

is the dielectric constant of free space. In the solution of the wave equation for E as given by equation (2.2), the first term represents a wave with magnitude E_1 traveling in the positive z direction, and the second term represents a wave with magnitude E_2 traveling in the negative z direction.

Now consider a inhomogeneous dielectric, where k varies with distance such that

$$k = \sqrt{\mu \varepsilon_o \varepsilon_r(z)} \tag{2.4}$$

and equation (2.2) is no longer valid. The solution cannot be conveniently expressed as a forward and backward traveling wave as for the homogeneous dielectric. As shown later in Section 3, except for certain special cases such as a linear dependence of ε with z (see section 3.2), to find a solution for the electric field in an inhomogeneous dielectric, equation (2.1) must be solved numerically.

2.2 Properties of Plasma

Let us consider the particular properties of a partially ionized, but electrically neutral, gas insofar as they affect the propagation of electromagnetic waves. Electrons have a natural frequency of oscillation called the plasma electron frequency or more commonly, the plasma frequency. It is represented by ω_N and is defined as follows [8]:

$$\omega_N^2 = \frac{N_e e^2}{\varepsilon_o m_e} \quad , \tag{2.5}$$

where ε_o is the permittivity of a vacuum, m_e is the mass of

an electron, N_e is the electron density, and e is the charge of an electron.

If temperature effects are not important, a plasma can be modeled as a dielectric as shown in reference 6, where

$$\varepsilon_r = 1 - \frac{\omega_N^2}{\omega^2} \quad , \tag{2.6}$$

ω is the transmitted frequency. In the general case ω_N can be a function of position, thereby, representing a inhomogeneous plasma. The refractive index of the ionized medium is given by [5]

$$n = (\varepsilon_r)^{\frac{1}{2}} = \left(1 - \frac{\omega_N^2}{\omega^2} \right)^{\frac{1}{2}} \quad . \tag{2.7}$$

Two cases are possible:

Case 1

$$\omega > \omega_N \qquad 1 - \frac{\omega_N^2}{\omega^2} > 0 \qquad n \text{ is real}$$

In this case, wave propagation takes place.

Case 2

$$\omega \leq \omega_N \qquad 1 - \frac{\omega_N^2}{\omega^2} \leq 0 \qquad n \text{ is imaginary}$$

In this case, the fields are evanescent and no wave propagation occurs. For a signal to be transmitted through a plasma it is, therefore, necessary that the frequency of the microwave signal ω be higher than the plasma frequency ω_N.

A wave, therefore, may propagate into a medium having increasing ω_N, but as ω_N approaches ω, $\varepsilon_r$approaches zero and a criterion for reflection is met. The point at which the electron density level causes the plasma frequency ω_N to equal ω is termed the turning point in this paper. To further illustrate the definition of turning point, in figure 1 the number N_e of free electrons per unit volume increases slowly in magnitude, reaches a maximum, and then falls abruptly with further increase in distance. A wave of a given frequency ω would enter the plasma without reflection because of the slow change in N_e. When the density N_e is large enough, however, $\omega_N(h_1) \cong \omega$. Then the dielectric constants in equation (2.6) vanish and the wave is reflected. In figure 1, h_1 is the location of the turning point.

2.3 Reflections

In the previous section, the properties of plasma were studied, and it was stated that a plasma can be modeled as a inhomogeneous dielectric. To understand reflections in a plasma, a formula for the reflection coefficient must be developed. Before we investigate reflections in the inhomogeneous dielectric model for the plasma we should examine a homogeneous dielectric. Consider a homogeneous dielectric with relative permittivity ε_r, a plane uniform wave progressing in the z-direction and having its electric vector in the y-direction is completely specified by equation (2.2) as

$$E_y(z) = E_1 e^{ikz} + E_2 e^{-ikz} \qquad (2.8)$$

where k is the wavenumber defined by equation (2.3) as

$$k = \sqrt{\mu \varepsilon_r \varepsilon_o} \quad . \tag{2.9}$$

The reflection coefficient at a location z_o can be defined as a complex number [9]

$$\Gamma(z_o) = \frac{E_2 e^{-ikz_o}}{E_1 e^{ikz_o}} \quad . \tag{2.10}$$

With equation (2.10), equation (2.8) can be written about the point z_o as

$$E_y(z) = E_i \left[e^{ik(z-z_o)} + \Gamma(z_o) e^{-ik(z-z_o)} \right] \quad , \tag{2.11}$$

where $E_i = E_1 e^{ikz_o}$ is the incident field for the traveling wave at z_o. Taking the derivative with respect to z, equation (2.11) becomes

$$\frac{\partial E_y(z)}{\partial z} = E_i \left[ike^{ik(z-z_o)} - ik\Gamma(z_o) e^{-ik(z-z_o)} \right] \quad . \tag{2.12}$$

We define a quantity p at the point z_o as

$$p = \frac{\frac{\partial E_y(z_o)}{\partial z}}{E_y(z_o)} \quad . \tag{2.13}$$

This factor p is proportional to the admittance of the wave given by H_x/E_y, where H_x is the magnetic field in the x direction. The resultant equation for the reflection coefficient at the location z_o can be written, in terms of p, as

$$\Gamma(z_o) = \frac{ik-p}{ik+p} \quad . \tag{2.14}$$

For values of p where the magnitude of Γ is zero in equation (2.11), the wave simply propagates in the +z direction with magnitude E_i. For values of p where the magnitude of Γ is unity, the wave is reflected and travels in the -z direction with magnitude E_i.

Having considered a homogeneous dielectric, we can investigate the inhomogeneous dielectric model for the plasma. As mentioned in section 2.1, equation (2.8) is not valid for inhomogeneous media and reference is made to the original Helmholtz wave equation. The Helmholtz wave equation is written here as

$$\frac{\partial^2 E_y(z)}{\partial z^2} + \omega^2 \mu \varepsilon(z) E(z) = 0 \quad . \tag{2.15}$$

As noted earlier for arbitrary variation of ε with z, it is not possible to find unique forward and backward waves in

equation (2.15). However, the kinds of variation of ϵ with z are such that there is a region of constant permittivity (free space) near the transmitting source. It is only in such a region of constant ϵ that equation (2.14) is actually evaluated after having found $E_y(z)$ everywhere using equation (2.15). Note that this wave equation has many solutions and equation (2.8) is a solution for a homogeneous medium only. To apply this equation for an arbitrarily varying dielectric, a solution must be found numerically for the ratio of the field expressions in equation (2.13) and subsequently for the reflection coefficient in equation (2.14) (see section 3.3). When the reflection coefficient for the modeled plasma is calculated at several frequencies, the frequency response for the plasma is known for that frequency range and the frequency response data can then be transformed to produce the time domain response for the plasma.

SECTION 3
REFLECTION COEFFICIENTS FOR UNIFORM, LINEAR, AND ARBITRARY INHOMOGENEOUS LAYERS

3.1 Uniform Dielectric Layer

Consider a plane wave incident on a plane uniform dielectric layer as shown in figure 3. The incident electric field which is polarized in the y-direction propagates in the z-direction through free space (Region I) and is normally incident on the layer (Region II) backed by free space (Region III). Normal incidence was chosen to simplify the problem. The electron density profile for the three regions is shown in figure 4. In free space (Regions I and III) the electron density is assumed to be zero, and for the dielectric layer (Region II), extending from $z=z_1$ to $z=z_2$, it is assumed to be N_o. The relative permittivity of the layer ε_d can be expressed by equations (2.5) and (2.6) as

$$\varepsilon_d = 1 - \frac{N_o e^2}{\omega^2 \varepsilon_o m_e} \qquad (3.1)$$

N_o is chosen so that $\omega_N > \omega$ and therefore $\varepsilon_d < 0$. The relative permittivity for this geometry is shown in figure 5. The field in Region III can be written with unity magnitude as

$$E(z) = e^{ik_o z} \qquad (z \geq z_2) \qquad (3.2)$$

[2] Electron density profile consistent with experimental predictions (see figure 2).

and

$$\frac{\partial E(z)}{\partial z} = ik_o e^{ik_o z} \qquad (z \geq z_2) \quad . \tag{3.3}$$

At $z=z_2$, the field can be written as

$$E(z_2) = e^{ik_o z_2} \tag{3.4}$$

and

$$\frac{\partial E(z_2)}{\partial z} = ik_o e^{ik_o z_2} \quad . \tag{3.5}$$

In Region II,

$$k = k_o \sqrt{\varepsilon_d} \tag{3.6}$$

and the index of refraction, n can be written as [9]

$$n = \sqrt{\varepsilon_r} = \sqrt{\varepsilon_d} \tag{3.7}$$

where ε_r is the relative permittivity. In general let

$$\sqrt{\varepsilon_r} = n_r + in_i \tag{3.8}$$

where n_r and n_i are the real and imaginary part of the index of refraction, respectively. Since n is purely imaginary for the relative permittivity here,

$$k = ik_o n_i \quad . \tag{3.9}$$

The field in Region II can be written as

$$E(z) = C_1 e^{ikz} + C_2 e^{-ikz} \qquad (z_1 \leq z \leq z_2) \quad . \tag{3.10}$$

Using equation (3.9), equation (3.10) can be written as

$$E(z) = C_1 e^{-k_o n_i z} + C_2 e^{k_o n_i z} \qquad z_1 \leq z \leq z_2 \tag{3.11}$$

and

$$\frac{\partial E(z)}{\partial z} = -k_o n_i C_1 e^{-k_o n_i z} + k_o n_i C_2 e^{k_o n_i z} \quad . \tag{3.12}$$

Using the boundary conditions, the tangential electric and magnetic fields are continuous at the interface $z=z_2$, we can equate the field expressions in equations (3.2) and (3.11), and equations (3.3) and (3.12), respectively, to solve for C_1 and C_2 (see reference 2). Note that

$$\frac{C_2}{C_1} = \frac{1 - \frac{1}{in_i}}{1 + \frac{1}{in_i}} e^{-2n_i k_o z_2}$$

will be very small if $n_i z_2$ is several free space wavelengths. Choosing z_2 such that $k_o n_i (z_2 - z_1) \gg 1$ renders $|C_2| \ll |C_1| e^{-2n_i k_o z_1}$. Similiarly, in Region I we can equate field expressions at $z=z_1$ and the reflection coefficient at $z=0$ can be written as (see reference 2)

$$\Gamma(z=0) = \frac{C_4}{C_3} \tag{3.13}$$

where

$$C_3 = \frac{n_i}{2i} \left[C_2 \left(1 - \frac{1}{in_i}\right) e^{k_o n_i z_1 (1 + \frac{1}{in_i})} - C_1 \left(1 + \frac{1}{in_i}\right) e^{-k_o n_i z_1 (1 - \frac{1}{in_i})} \right] \tag{3.14}$$

and

$$C_4 = \frac{n_i}{2i} \left[-C_2 \left(1 + \frac{1}{in_i}\right) e^{k_o n_i z_1 (1 - \frac{1}{in_i})} + C_1 \left(1 - \frac{1}{in_i}\right) e^{-k_o n_i z_1 (1 + \frac{1}{in_i})} \right] . \tag{3.15}$$

Since $|C_2| \ll |C_1| e^{-2n_i k_o z_1}$,

$$\Gamma(z=0) = \frac{1-in_i}{1+in_i} e^{2ik_o z_1} \quad , \qquad (3.16)$$

where

$$n_i = \sqrt{|\epsilon_d|} \qquad (3.17)$$

3.2 Linear Layer

In the previous section we calculated the complex reflection coefficient for a uniform dielectric layer. Now consider a linear layer as shown in figure 6. A plane wave, polarized in the y-direction and traveling in the z-direction through free space (Region I, $N_e=0$), is incident on the layer at $z=z_1$. As the wave progresses through the layer (Region II), it encounters greater electron densities. At the outer edge of the layer, $z=z_2$, the electron density N_e is at its maximum, N_o. As the wave leaves the layer, it returns to free space (Region III, $N_e=0$). The electron density profile can be expressed as

$$N_e = \frac{N_o}{z_2-z_1} z - \frac{N_o z_1}{z_2-z_1} \qquad (z_1 \leq z \leq z_2) \qquad (3.18)$$

and in air as

$$N_e = 0 \qquad (z \leq z_1 \text{ and } z \geq z_2). \qquad (3.19)$$

When the electron density N_e is large enough, the relative dielectric constant ε_r in equation (3.1) vanishes and the wave is reflected. Let us call this critical electron density value N_c. For the dielectric constant to vanish

$$N_c = \frac{\omega^2 \varepsilon_o m_e}{e^2} \quad . \tag{3.20}$$

By using equation (3.18) we find this to happen at the turning point

$$z = z_1 + \frac{\omega^2 \varepsilon_o m_e \Delta z}{N_o e^2} \tag{3.21}$$

where

$$\Delta z = z_2 - z_1 \quad . \tag{3.22}$$

The field in Region III can be written with unity magnitude as

$$E(z) = e^{ik_o z} \qquad (z \geq z_2) \tag{3.23}$$

and

$$\frac{\partial E(z)}{\partial z} = ik_o e^{ik_o z} \qquad (z \geq z_2) \quad . \tag{3.24}$$

In Region II the Helmholtz wave equation derived in reference 9 becomes the Airy differential equation as shown in reference 2. The field expressions can then be written in terms of Airy functions (see reference 2) as

$$E(u) = C_1 Ai(u) + C_2 Bi(u) \tag{3.25}$$

and

$$\frac{\partial E(u)}{\partial u} = C_1 \frac{\partial}{\partial u} Ai(u) + C_2 \frac{\partial}{\partial u} Bi(u) \tag{3.26}$$

where the variable u(z) is defined as

$$u(z) = -\left[\frac{k_o^3 \, \Delta z}{K_1}\right]^{\frac{2}{3}} \left[1 - \frac{K_1}{k_o^2}\left[\frac{z-z_1}{\Delta z}\right]\right] \tag{3.27}$$

and

$$K_1 = \frac{N_o e^2}{c^2 \varepsilon_o m_e} \tag{3.28}$$

Using the boundary conditions at $z=z_1$ and $z=z_2$, we can equate field expressions and solve for the reflection coefficient at z=0 (see reference 2). At z=0 we are in free space, a region of constant permittivity, the reflection coefficient at z=0 can be written as

$$\Gamma(z=0) = \frac{\left[C_1 L_1 + C_2 L_2 \right] e^{2ik_o z_1}}{C_1 L_3 + C_2 L_4} \tag{3.29}$$

where

$$L_1 = Ai(u(z_1)) - \frac{\frac{\partial}{\partial u}Ai(u(z_1))}{ik_o \frac{\partial z}{\partial u}} \tag{3.30}$$

$$L_2 = Bi(u(z_1)) - \frac{\frac{\partial}{\partial u}Bi(u(z_1))}{ik_o \frac{\partial z}{\partial u}} \tag{3.31}$$

$$L_3 = Ai(u(z_1)) + \frac{\frac{\partial}{\partial u}Ai(u(z_1))}{ik_o \frac{\partial z}{\partial u}} \tag{3.32}$$

$$L_4 = Bi(u(z_1)) + \frac{\frac{\partial}{\partial u}Bi(u(z_1))}{ik_o \frac{\partial z}{\partial u}} \tag{3.33}$$

To illustrate this exact solution for the reflection coefficient, a particular linear profile was chosen and is shown in figure 7. The electron density N_e begins at the front interface, z=0, at a value of zero and rises to a value of $1x10^{20}$ electrons per cubic meter at z=14 centimeters (the exit point). The real and imaginary parts of the reflection coefficient at the front interface are shown in the right column in table I for 74 to 75 GHz.

3.3 Plasma Layer

In the two previous sections the complex reflection coefficients for a constant dielectric slab and a linear layer were derived exactly. The solution for an arbitrary inhomogeneous plasma layer requires, in general, numerical techniques. The plasma is represented by a

scalar, isotropic, and inhomogeneous dielectric constant. Consider a plasma layer with a electron density profile as shown in figure 2. An incident electric field, which is polarized in the y-direction, propagates in free space (Region I), in the z-direction, and is normally incident on the plasma layer (Region II) and backed by free space (Region III) as shown in figure 8. Again, normal incidence was chosen to simplify the problem of studying the effects of electron density fluctuations on the time-domain reflectometer response for a one-dimensional plasma sheath.

The Helmholtz wave equation for the electric field in a inhomogeneous plasma layer is written as

$$\frac{\partial^2 E_y(z)}{\partial z^2} + k^2(z) E_y(z) = 0 \qquad (3.34)$$

where k, the wavenumber, is

$$k(z) = \omega \sqrt{\mu\varepsilon(z)} \quad . \qquad (3.35)$$

The wave propagates through the plasma (Region II) and is transmitted to free space (Region III). Since the relative dielectric constant in free space equals one, the solution of equation (3.34) in Region III is readily found.

To begin the solution, the electric field in Region III may again be written with unity magnitude as

$$E_y(z) = e^{ik_o z} \quad . \qquad (3.36)$$

The derivative needed to define p in equation (2.13) is again given by

$$\frac{\partial E_y(z)}{\partial z} = ik_o e^{ik_o z} \quad . \tag{3.37}$$

The field at z=d is assumed to be unity and, therefore, can be written as

$$E_y(z=d) = e^{ik_o d} \tag{3.38}$$

and

$$\frac{\partial E_y(z=d)}{\partial z} = ik_o e^{ik_o d} \quad . \tag{3.39}$$

Equations (3.38) and (3.39) serve as boundary conditions for solving equation (3.34). Dropping the polarization notation and making the substitution

$$S(z) = \frac{\partial E(z)}{\partial z} \tag{3.40}$$

equation (3.34) becomes

$$\frac{\partial S(z)}{\partial z} + k^2(z)E(z) = 0 \quad . \tag{3.41}$$

Using a fourth-order Runge-Kutta method [10], equations (3.40) and (3.41) can be integrated to find the electric field and its derivative. Once these are found at z=0, p at

z=0 becomes

$$p = \frac{\frac{\partial E(z=0)}{\partial z}}{E(z=0)} \qquad (3.42)$$

as defined by equation (2.13) and the reflection coefficient at z=0, in terms of p, is

$$\Gamma(z=0) = \frac{ik-p}{ik+p} \qquad (3.43)$$

One can note that only the ratio of S(z) to E(z) is actually needed to compute the reflection coefficient. Thus, the magnitude of E(z) can be kept near unity by normalizing the solution at the end of each Runge-Kutta step.

3.4 Verification of Runge-Kutta Method

In section 3.2, a linear profile was chosen to demonstrate an exact method (Airy-equation) of determining the reflection coefficient. A comparison of the numerical Runge-Kutta solution and this exact solution is made. The particular linear profile chosen is shown in figure 7. The real and imaginary parts of the reflection coefficient at the front interface for the Runge-Kutta method and the exact method are shown in table I for 74 to 75 GHz. The Runge-Kutta method compares favorably with the exact solution as can be readily seen in table I. In all cases, the number of Runge-Kutta steps used was tested so that significant changes in computed values were not observed for

larger numbers of steps.

SECTION 4
TIME DOMAIN MEASUREMENTS

4.1 Uniform Dielectric Layer

As stated, the complex reflection coefficient, for a range of constituent transmitted microwave frequencies, can be used to synthesize the effective time domain response of a plasma layer (see Appendix for a review of time domain theory). Sixty four frequencies, for a bandwidth of 2 GHz, were chosen to be consistent with the MRIS experiment. Reflection coefficient data in the frequency domain are shifted and transformed to give a baseband time domain response using a decimation-in-time fast inverse Fourier transform [11]. The resulting time domain response emulates a baseband continuous wave signal, where the peak magnitude marks the location of the turning point. The frequency domain data are windowed by a Kaiser-Bessel window to reduce unwanted interference, and it should be noted that the peak response of the data is normalized to the reponse of the window. To illustrate the technique of using the time domain response to locate the turning point, the results of section 3.1 are used for a uniform dielectric layer.

Consider a plane wave incident on a uniform dielectric slab, with $\epsilon_r = -0.5$, located 10 cm from the source, as shown in figure 5. A negative permittivity was chosen to simulate a purely reactive dielectric reflector. The wave propagates through free space (Region I) at the speed of light c and is normally incident on the slab at $z_1 = 10$ centimeters. The slab is 14-cm thick (Region II) and is backed by free space (Region III). As stated by equation (2.10), the ratio of the amplitude of the field reflected by the dielectric slab

to the amplitude of the field incident at $z=z_1$ is called the reflection coefficient Γ of the uniform dielectric slab. We should note by equation (3.16) that Γ is the reflection coefficient pertaining to $z=0$ and takes into account the effect of the propagation path from 0 to z_1. The effects of the back of the slab are attenuated and not seen. The wave is incident and reflected at the $z=z_1$ interface, which is the turning point for the dielectric layer. The magnitude and phase of the reflection coefficient for the uniform dielectric layer are shown in figures 9 and 10, respectively, for 74 to 76 GHz. The phase plot is relative to the phase at 74 GHz. These reflection coefficient data were transformed and windowed with the resulting time domain response of the layer as shown in figure 11. The response is shifted to the left of time t=0 and the shift is the propagation delay of the wave. Note that this delay is measured on the negative side of the time axis and has negative values. Due to the truncated frequency domain, ringing is associated with the time domain response. A Kaiser-Bessel window [10] was chosen and the frequency data were multiplied by the real Kaiser-Bessel weights to emulate a pulse train with very low sidelobes or "ringing" between pulses. Sidelobes can limit the dynamic range of the time domain measurement by hiding low-level responses within the sidelobes of the higher level responses.

To estimate the location of the turning point, the time for the wave to travel to the turning point had to be determined. The time domain response was used to calculate this propagation time. In figure 12, we see the transformed reflection coefficient for -2 to 2 nanoseconds plotted with the effective transmitted pulse (i.e., the transformed Kaiser-Bessel window) as a reference centered at t=0. The time shift between the two plots corresponds to the round-trip propagation delay for the wave and is labeled

$2t_d$, where t_d is the one-way propagation delay measured on the negative side of the time axis. Since the wave traveled at the speed of light c in Region I and t_d was measured to be .3352 nanoseconds, the wave traveled 10 cm before it was reflected. This is in agreement with the geometry of the problem, where the turning point is located at $z=z_1$ (z_1=10 cm).

4.2 Plasma Layer

For the plasma layer the turning point is located within the layer. To estimate the turning point distance, the velocity through the plasma must be obtained. This suggests a problem since the plasma is modeled as a inhomogeneous dielectric and the velocity of the propagating wave is dependent on the permittivity of the medium. Some means must be found to approximate the velocity profile. A possible solution is to assume that regions of the plasma profile are piecewise linear to find average velocities for each such region. To approach this problem, let us look at the linear layer discussed in section 3.2. The electron density profile of the layer bounded on both sides by free space is shown in figure 6. The phase velocity through the layer is

$$v_p(z) = \frac{c}{\sqrt{\epsilon_r(z)}} \quad . \tag{4.35}$$

The group velocity which describes the transport of energy is related to the phase velocity and is

$$v_g(z) = \frac{c^2}{v_p(z)} \quad . \tag{4.36}$$

At the front interface of the layer ($z=z_1$) the relative permittivity is that of free space and is equal to one. The group velocity there is simply the speed of light c. As the wave travels through the layer, it encounters greater electron density N_e values and its group velocity decreases. When the electron density is large enough, the relative dielectric constant ε_r vanishes in equation (2.6) and the phase velocity becomes infinite forcing the group velocity in equation (4.36) to become zero. Note that this occurs at the turning point. It is, therefore, possible to assume that the average group velocity, as the wave propagates from the front interface to the turning point, is c/2. For investigations of wave propagation in a linear layer plasma, such an assumption is, therefore, quite permissible. However, as the plasma becomes nonlinear, the c/2 assumption becomes less accurate.

To illustrate this point, shown in figure 2 is an electron density profile which is consistent with the MRIS experiment that is being simulated. As an example, let us assume the profile to be linear for electron densities less than $1.00\text{x}10^{14}/\text{cm}^3$. We will assume this to be true only for this region in order to derive an average group velocity for the region. Note that for electron densities less than $1.00\text{x}10^{14}/\text{cm}^3$ the critical frequency is less than 90 GHz by equation (2.5). For this region, as before, the average group velocity is approximated as c/2. For 74 to 76 GHz, the time domain response was obtained. With this result, the turning point was estimated at .77 cm. This is in reasonable agreement with the exact location of .87 cm . It should be emphasized that this approach was given here as an

example and that a better approximation could be made by further segmenting the same region to find more accurate velocity values. Such further segmenting would require additional measurements at frequencies below 74 GHz.

SECTION 5
PLASMA FLUCTUATIONS

5.1 Background

In the previous chapter we synthesized the effective time domain reflectometry response of a plasma using a range of transmitted microwave frequencies. These results as a whole gave us an estimate for the location of the critical electron densities in static plasma models. However, macroscopic effects of electron density fluctuations, which are not included in standard aerothermodynamic simulations, may have a noticeable effect on hypersonic reentry flow fields [12]. In order to monitor these effects, we will extend the foregoing discussion on the propagation of waves through static plasma models. Thus, we consider the important effects of time-dependent electron density fluctuations on the time domain response of a plasma.

Fluctuation of the profile results in motion of the turning point and is emulated between frequency step measurements. Motion occurs between frequency step measurements, assuming that each individual measurement is accurate at each step. Two Doppler effects resulting in motion are studied; the first type of motion involves reducing the electron density profile while preserving the shape of the profile and the second type of motion involves modulating the density profile. The first effect is demonstrated in figure 13 where a sample electron density profile is reduced, moving the turning point from h_1 to h_2 and then h_3. The second effect can be seen in figure 14 after the same electron density profile is modulated. Two different rippled profiles are shown moving the turning point from d_1 to d_2. Both effects are applied

incrementally between frequency steps and consequently results in erratic motion of the turning point. The nonuniform motion of the turning point is estimated by calculating the location of the turning point at specific times during the measurement period. These discrete calculations give an indication of the overall motion of the turning point caused by the two effects. Turning point velocities achieved are significantly less than predicted flow field Mach velocities of hypersonic reentry vehicles [13].

5.2 Reduction of Electron Density Profile

The first type of motion resulted by reducing the given electron density profile values of figure 2 by percentages without changing the shape of the profile. Shown in figure 15 are the time domain responses for three electron density profiles for 74 to 76 GHz. Time t=0 corresponds to the location of the time domain response of the window used. The first profile has 100 percent density values, the second has 95 percent values and the third has 90 percent values. It is evident that the responses shift toward the left, moving the turning point left of time t=0, with decreasing percentages. To understand the displacement of the turning point, the location of the turning point was calculated for the 100 percent case and the 90 percent case at 75 GHz. By using equations (2.5) and (2.6), the turning point moved .13 cm for the 10 percent variation in the profile. Using the dwell time of 2.5 milliseconds for the proposed MRIS instrument[3], a turning point velocity of .52 meters per second was computed.

[3]MRIS Experiment Requirements Document (ERD)

To emulate a moving profile response, where the turning point moves as the frequency is stepped from 74 to 76 GHz, the profile was reduced from 100 percent to 90 percent. The time domain response for this emulated variation in the profile is shown in figure 16, left of a static 95 percent profile response. The 95 percent profile response is considered to be the response at which the turning point is at its average position for the 10 percent variation in the profile. A shift between this average and emulated response of .17 nanoseconds was computed. By using an average velocity of c/2, the turning point was found to have shifted 1.28 cm in comparison to the variation in the static profile turning point of .13 cm. This significant increase in profile shift due to the media motion is a major potential error.

5.3 Modulation of Electron Density Profile

For the second type of motion investigated, modulation was introduced into the profile. An expression is written in the form

$$1 + A \cos(Kz + \psi) \tag{5.1}$$

where A is the amplitude, ψ is the phase of the modulating wave, and K is the spatial wavenumber defined as

$$K = \frac{2\pi}{\chi} \quad , \tag{5.2}$$

where χ is the spatial wavelength. This function was used to modulate the profile. By varying the phase ψ of this

function, the disturbance described by equation (5.1) was set into motion and traveled across the profile.

A modulating wave with an amplitude of .05 and a wavelength of 2 cm was chosen. To mimic a modulation velocity of 2 meters per second, the phase ψ of equation (5.1) was varied from 0° to 90° as the frequency was stepped from 74 to 76 GHz. The time domain response is shown in figure 17. By squaring the transform reflection coefficient in figure 17, the power distribution in the time domain can be viewed. The power distribution for the response in figure 17 is shown in figure 18. Greater modulation velocities up to 8 meters per second were investigated and results for the reflection coefficient and the power distribution are shown in figures 19 and 20, respectively. Further work was done for 140 to 142 GHz with the same modulating wave to illustrate greater effects at higher frequencies, the transform reflection coefficients were determined, and the associated power distributions are shown in figures 21 and 22. In addition, for 74 to 76 GHz the amplitude of the modulation was raised to .25 and results are shown in figures 23 through 25.

Smearing and shifting of the time domain reconstruction is quite evident for the cases studied. For example, at 140 to 142 GHz the response maximum moved from -1 nanoseconds to -2.4 nanoseconds as the modulation velocity was increased from .22 meters per second to 3.33 meters per second (see figures 21 and 22), and as the velocity was increased further to 8 meters per second, the response became more smeared and shifted with multiple echoes (see figure 22d). Various methods for finding the turning point from these responses can be employed. Two approaches are presently realizable; one approach involves finding the peak power level and designating it as the location of the turning point and another approach involves finding the centroid of the

area under the power distribution plot, where the centroid would mark the location of the turning point. There are a few problems with these approaches. Smearing of the time domain response results in several peaks which may be used to define the turning point, limiting the accuracy of the first approach. Shifting of the response centroid would also limit the success of the centroid approach. Using the previous example for 140 to 142 GHz, the centroid of the distribution moves from -1 nanosecond to -2.6 nanoseconds as the modulation velocity is increased from .22 to 3.33 meters per second.

From the results presented, a limitation of 2.67 meters per second on the turning point velocity is estimated for the accuracy of the instrument at 140 to 142 GHz with modulation amplitude A=.05. For 74 to 76 GHz with modulation amplitude A=.25, it is estimated that there is potential error with turning point velocities greater than 4.67 meters per second.

The following conclusions should be kept in mind when assessing the location of the turning point:

1. Amplitude fluctuations in the electron density profile cause a shift or delay in the effective time domain response.
2. Smearing of the time domain response, creating multiple peaks, becomes significant for rapid fluctuations in the electron density profile.
3. Strategies for locating the turning point can be chosen to possibly minimize adverse effects resulting in shifting and smearing of the time domain response.

SECTION 6
CONCLUDING REMARKS

The results of studying the effects of moving electron density fluctuations on frequency generated time-domain reflectometry in a one-dimensional plasma layer have been presented. On the basis of the studies made and the data obtained, the following remarks and conclusions may be made:

(a) Different models for a plasma layer have been developed and discussed in length.

(b) Equations describing wave propagation through different plasma models have been formulated.

(c) The computer program synthesizes, using 64 frequencies, the time domain response of a given plasma electron density profile. A linear profile with an exact solution (Airy solution) compared accurately with the program's numerical Runge-Kutta solution. A uniform dielectric slab with a known turning point was also used successfully to verify the code.

(d) The average velocity of an electromagnetic wave propagating through plasma must be accurately estimated to determine the location of critical electron densities.

(e) Varying electron density levels corrupt time domain and distance measurements. In this work it has been shown that lowering or reducing the electron density levels of a given electron density profile, while maintaining the shape of the profile as in figure 13,

results in motion of the turning point, and the effective motion has a significant effect on measuring critical electron density locations.

(f) Modulating an electron density profile with a waveform creates a disturbance or ripple adversely affecting the time domain response of a plasma. Waveforms with phase variations emulating motion across the profile were used and greatly influenced simulated measurements, especially for rapid phase variations.

(g) A technique such as the centroid method for locating the turning point may be used to reduce the effects of electron density fluctuations on turning point estimates.

All of these issues, and perhaps more which now remain unidentified, must be addressed and quantified in order to arrive at an estimate of the usefulness of time domain reflectometry for locating critical electron densities in plasma.

A 10 percent reduction of the electron density profile as described in section 5.2 shifts the turning point significantly and may contribute to error. By modulating the electron density profile as in section 5.3, there is a potential for error when turning point velocities greater than 2.67 meters per second are achieved at 140 to 142 GHz with modulation amplitude A=.05. For 74 to 76 GHz with modulation amplitude A=.25, turning point velocities greater than 4.67 meters per second may also induce errors. It must be concluded that a distance-measuring scheme using time domain reflectometry (i.e., MRIS) could become inaccurate if some of the plasma fluctuations investigated in this paper are encountered. It has been the intent of this paper to

help identify and possibly solve similar induced errors should they occur.

Appendix

Time Domain Theory

Time domain theory plays an important role in the MRIS distance-measuring technique. The response of plasma to a time domain signal is used to estimate distances to critical electron densities. Plasma reflection information in the frequency domain is taken and transformed to the time domain where propagation delays are measured to calculate these distances. In this process, a frequency down conversion takes place so that the resulting time domain response emulates a baseband continuous wave signal. Further, an I,Q (In-phase, Quadrature) detector is used to construct the time domain signal. Processing of this signal is done in the form of windowing to reduce unwanted interference.

To understand exactly how an I,Q detector can obtain a time domain response by only using discrete samples of amplitude and phase in the frequency domain, consider first the problem in reverse. Let a transmitted periodic pulse train in the time domain be represented by the signal

$$f(t) = \sum_{n=M}^{M+k} a_n e^{-in\omega_o t} + \sum_{n=-M}^{-(M+k)} a_n e^{-in\omega_o t} \qquad (A.1)$$

with

$$\omega_o = 2\pi/T_o \qquad (A.2)$$

where a_n is complex and T_o is the period. The signal is real and periodic with 2k spectral components, where k is the number of spectral lines in the positive or negative

frequency domains. The amplitude spectrum starts with a_M in the positive frequency domain and a_{-M} in the negative frequency domain. M is chosen here as an arbitrary constant. Let n=-n in the second summation and drop the primes. The signal becomes one summation

$$f(t) = \sum_{n=M}^{M+k} \left[a_n e^{-in\omega_o t} + a_{-n} e^{in\omega_o t} \right] \quad . \qquad (A.3)$$

Let $a_{-n} = a_n^*$ so that f(t) is real, then

$$f(t) = \sum_{n=M}^{M+k} \left[(a_n + a_n^*)\cos\, n\omega_o t - i(a_n - a_n^*)\sin\, n\omega_o t \right] \quad . \qquad (A.4)$$

Further, let

$$A_n = a_n + a_n^* \qquad (A.5)$$

and

$$B_n = i\left[a_n - a_n^* \right] \quad . \qquad (A.6)$$

To make a frequency down coversion of the signal we start by introducing the sinusoidal tone cos $p\omega_o t$. For any p where

$$M \leq p \leq M+k \quad \text{and} \quad k < M$$

multiply both sides by cos $p\omega_o t$, thus

$$f(t)\cos\ p\omega_o t = \sum_{n=M}^{M+k}\Big[A_n(\cos\ n\omega_o t\cdot\cos\ p\omega_o t) - B_n(\sin\ n\omega_o t\cdot\cos\ p\omega_o t)\Big]$$

$$= \sum_{n=M}^{M+k}\left[\frac{A_n}{2}\left[\cos(n-p)\omega_o t + \cos(n+p)\omega_o t\right] - \frac{B_n}{2}\left[\sin(n+p)\omega_o t + \sin(n-p)\omega_o t\right]\right]. \tag{A.7}$$

Low pass filtering this response for frequencies less than $2M\omega_o$) we obtain a filtered version of $f(t)\cos\ p\omega_o t$ as

$$\text{LPF}\left[f(t)\cos\ p\omega_o t\right] = \sum_{n=M}^{M+k}\left[\frac{A_n}{2}\cos(n-p)\omega_o t - \frac{B_n}{2}\sin(n-p)\omega_o t\right]. \tag{A.8}$$

where LPF denotes the low-pass filtering. The frequencies present range from 0 to $k\omega_o$.

Now let $f(t)\cos\ p\omega_o t$ be placed in a narrow band low pass filter such that frequencies of ω_o and above are completely cut off. Then all of the terms in the summation except for n=p are suppressed and

$$\text{BPF}\left[f(t)\cos\ p\omega_o t\right] = \frac{A_p}{2} \quad . \tag{A.9}$$

where BPF denotes the bandpass filter. This signal would be detected in the I (In-phase) channel of an I,Q synchronous detector with the heterodyne frequency being $p\omega_o$, or

equivalently in a homodyne synchronous detector if the signal f(t) represented a single frequency signal of frequency $p\omega_o$ rather than a pulse train signal.

To find the output of the Q (Quadrature) channel multiply f(t) by sin $p\omega_o t$. Similarly we find

$$f(t)\sin p\omega_o t = \sum_{n=M}^{M+k} \left[A_n \cos n\omega_o t \cdot \sin p\omega_o t - B_n \sin n\omega_o t \cdot \sin p\omega_o t\right]$$

$$= \sum_{n=M}^{M+k} \left[\frac{A_n}{2}\left[\sin(n+p)\omega_o t + \sin(p-n)\omega_o t\right] - \frac{B_n}{2}\left[\cos(p-n)\omega_o t - \cos(n+p)\omega_o t\right]\right] . \quad (A.10)$$

After filtering out frequencies less than $2M\omega_o$

$$\text{LPF}\left[f(t)\sin p\omega_o t\right] = \sum_{n=M}^{M+k} \left[\frac{A_n}{2}\sin(p-n)\omega_o t - \frac{B_n}{2}\cos(p-n)\omega_o t\right] \quad (A.11)$$

and after cutting off at ω_o and above

$$\text{BPF}\left[f(t)\sin p\omega_o t\right] = -\frac{B_p}{2} . \quad (A.12)$$

The quantity $-B_p/2$ is then the output of the Q channel. If

the medium (plasma) being probed is not dependent on time, then the sequence of, essentially d.c. measurements, A_p and B_p would be completely sufficient for the construction of $f(t)$.

With the construction of $f(t)$ by the I,Q detector, further processing is done to eliminate interference. To show how this is done, consider a real function, later to be called a "window" function

$$w(t) = \sum_{n=M}^{M+k} W_n \cos n\omega_o t \qquad (A.13)$$

and form another function

$$g(t) = \int_{-T_o/2}^{T_o/2} f(\tau)w(t-\tau)\, d\tau \qquad (A.14)$$

where

$$T_o = \frac{2\pi}{\omega_o} \quad \text{for all} \quad \frac{-T_o}{2} \le t \le \frac{T_o}{2} \; .$$

Let $g(t)$ be periodic with period T_o so that

$$g(t) = \int_{-T_o/2}^{T_o/2} \left[\sum_{n=M}^{M+k} A_n \cos n\omega_o\tau - B_n \sin n\omega_o\tau \right] \cdot \left[\sum_{m=M}^{M+k} W_m \cos m\omega_o(t-\tau) \right] d\tau$$

$$= \sum_{n=M}^{M+k} \sum_{m=M}^{M+k} \int_{-T_o/2}^{T_o/2} \left[\left(A_n W_n \cos\, n\omega_o\tau \cdot \cos\, m\omega_o(t-\tau) \right) - \left(B_n W_n \sin\, n\omega_o\tau \cdot \cos\, m\omega_o(t-\tau) \right) \right] d\tau \ . \tag{A.15}$$

The first term can be expanded where

$$\cos\, n\omega_o\tau \cdot \cos\, m\omega_o(t-\tau) = \cos\, m\omega_o t \left[\tfrac{1}{2}\cos(n-m)\omega_o\tau + \tfrac{1}{2}\cos(n+m)\omega_o\tau \right] + \sin\, m\omega_o t \left[\tfrac{1}{2}\sin(m+n)\omega_o\tau + \tfrac{1}{2}\sin(m-n)\omega_o\tau \right] \ . \tag{A.16}$$

Note that integration over a complete period τ causes all terms to vanish except those where m=n. Expansion of the second term in equation (A.15) gives a similar result. Thus,

$$g(t) = \frac{T_o}{2} \sum_{n=M}^{M+k} W_n \left\{ A_n \cos\, n\omega_o t - B_n \sin\, n\omega_o t \right\}. \tag{A.17}$$

multiplication term-by-term of the Fourier series representing f(t) by W_n, produces the Fourier series of g(t) given by equation (A.14). Thus, any pulse train described by a set of A_n's and B_n's and, hence, f(t) can be transformed into another pulse train with a differently shaped pulse by multiplying each term in the Fourier series by W_p.

As an example of how a signal f(t) is windowed, let a set of A_n's and B_n's be chosen arbitrarily and let $A_n=1/k$ for all $M \le n \le M+k$ and $B_n=0$ for all such n. Thus, using

equations (A.5) and (A.6) in equation (A.4) gives

$$f(t) = \sum_{n=M}^{M+k} \left(\frac{1}{k}\right) \cos\, n\omega_o t \quad . \tag{A.18}$$

Note that f(t) is clearly periodic with period $2\pi/\omega_o$ and has equally weighted spectral components. Consider the function f(t) for $-\pi/\omega_o \leq t \leq \pi/\omega_o$. In order to illustrate the windowed function f(t), consider a limiting form for this function obtained by letting $\omega_o \to 0$, $M \to \infty$, $k \to \infty$ in a certain way so that the number of components in the spectrum becomes infinite. We first write

$$f(t) = \sum_{n=M}^{M+k} \left(\frac{1}{k}\right) \cos\, n\omega_o t = \sum_{n=M}^{M+k} \frac{\omega_o T_o}{\omega_o T_o k} \cos\, n\omega_o t \ , \tag{A.19}$$

so

$$f(t) = \frac{T_o}{2\pi k} \sum_{n=M}^{M+k} (\cos\, n\omega_o t)\omega_o \quad , \quad T_o = \frac{2\pi}{\omega_o} \quad . \tag{A.20}$$

Then let $\omega_o \to 0$, $M \to \infty$, $k \to \infty$ such that

$$n\omega_o = \omega \tag{A.21}$$

$$\omega_o = \Delta\omega \tag{A.22}$$

$$M\omega_o = \Omega_1 \tag{A.23}$$

$$(M+k)\omega_o = \Omega_2 \tag{A.24}$$

$$\frac{T_o}{k} = T = \frac{2\pi}{\Omega_2 - \Omega_1} \tag{A.25}$$

We can write $f_1(t)$ for this limiting case

$$f_1(t) = \frac{T}{2\pi}\int_{\Omega_1}^{\Omega_2} \cos\ \omega t\ d\omega \quad = \frac{T}{2\pi}\,\frac{1}{t}\left[\sin\ \Omega_2 t - \sin\ \Omega_1 t\right] \tag{A.26}$$

Now

$$\sin\ \Omega_2 t - \sin\ \Omega_1 t \equiv 2\left[\sin\left(\frac{\Omega_2-\Omega_1}{2}\right)t\right]\cos\ \frac{\Omega_2+\Omega_1}{2}\,t \quad , \tag{A.27}$$

so the limiting form of f(t) is

$$f_1(t) = \frac{T_o}{\pi}\left(\frac{\Omega_2-\Omega_1}{2}\right)\left[\frac{\sin\ \frac{\Omega_2-\Omega_1}{2}\,t}{\frac{\Omega_2-\Omega_1}{2}\,t}\right]\cos\ \frac{\Omega_2+\Omega_1}{2}\,t \quad , \tag{A.28}$$

a carrier at $(\Omega_1+\Omega_2)/2$ modulated by a sinc function whose first zero is at $t = 2\pi/(\Omega_2-\Omega_1)$. The limiting form of the pulse in equation (A.28) may be repeated such that $f(t+nT_o) \simeq f(t)$ for all integer n. In reality this limiting form of the pulse shape is not achieved. We must really deal with the finite sum and finite ω_o of equation (A.18). Thus, the "sinc" modulation is only suggestive of what the actual pulse shape using finite ω_o will be.

The use of no window implies that we are using a pulse train exactly given by equation (A.18), which in the limiting case looks like a "sinc"-modulated carrier pulse train given by equation (A.28). Other shaped pulse trains can be produced by windowing f(t), to give

$$g(t) = \sum_{n=M}^{M+k} W_n \cdot \frac{1}{k} \cos\, n\omega_o t \quad . \qquad (A.29)$$

The Kaiser-Bessel set of frequency weights W_n gives a well defined pulse shape that is nearly zero over most of the T_o period except for the desired pulse itself. Equation (A.18) or (A.29) may be considered as the transmitted signal at some reference point (reference plane, antenna terminals, etc.). This transmitted signal will propagate into the plasma medium and result in a scattered electromagnetic field which will then appear at the same reference point. One should expect for a frequency dependent medium such as a plasma, that the scattered signal will be distorted as well as delayed with respect to the transmitted pulse train. The effect of the medium will appear in the measured reflection coefficient at the reference point for each constituent frequency in the signal. This set of reflection coefficients can be determined in principle by homodyne synchronous (I,Q) detection of the received signal at each of the stepped radio frequencies and normalization by the magnitude of the transmitted signal. The preceding discussion, thus, shows that the response of a time independent, but frequency dispersive plasma medium to a time domain pulse train signal, can be rigorously emulated by a sequence of frequency domain measurements taken one frequency at a time.

If R_n is the complex reflection coefficient at frequency $n\omega_o$, then the effective received time domain signal $f_R(t)$ due to equation (A.18) is

$$f_R(t) = \frac{1}{2}\sum_{n=M}^{M+k} R_n e^{-in\omega_o t} + \frac{1}{2}\sum_{n=-M}^{-(M+k)} R_n e^{-in\omega_o t}$$

$$= \sum_{n=M}^{M+k} |R_n| \cos(n\omega_o t + \phi_n)$$

where

$$\phi_n = \tan^{-1}\left[\frac{\text{Im}\ (R_n)}{\text{Re}\ (R_n}\right] \qquad (A.30)$$

Note that R_n is complex and that we take $R_{-n}=R_n*$. Thus, $f_R(t)$ is real. As written, equation (A.30) is the response of the medium to a pulse train that resembles the "sinc" modulated pulse train form of equation (A.28). A "window" sequence W_n can be applied at this point to give the received windowed signal f_{RW}, which may be written as

$$f_{RW}(t) = \frac{1}{2}\sum_{n=M}^{M+k} R_n W_n e^{-in\omega_o t} + \frac{1}{2}\sum_{n=-M}^{-(M+k)} R_n W_n e^{-in\omega_o t}$$

$$= \sum_{n=M}^{M+k} W_n\ |R_n| \cos(n\omega_o t + \phi_n) \quad , \qquad (A.31)$$

where ϕ_n is the same as in equation (A.30) and $W_n \equiv W_{-n}$. Note again that each R_n is measured essentially as a (complex) d.c. quantity even though the value of R_n is that appropriate for the response of the medium at frequency $n\omega_o$. Since we are interested primarily in the time delays associated with the received signals in order to measure distances to the turning point, we are not really interested

in the radio frequency behavior of $f_{RW}(t)$ of equation (A.31). Without any loss of desired information, we can set M=0 in equation (A.31) and emulate a baseband pulse train which represents the envelope of the received signal. The final version of the emulated received signal is a received, windowed, baseband signal f_{RWB}, written as

$$f_{RWB}(t) = \frac{1}{2}\sum_{n=0}^{k} \mathbb{W}_n \mathbb{R}_n e^{-in\omega_o t} + \frac{1}{2}\sum_{n=0}^{-k} \mathbb{W}_n \mathbb{R}_n e^{-in\omega_o t}$$

$$= \sum_{n=0}^{k} \mathbb{W}_n |\mathbb{R}_n| \cos(n\omega_o t + \Phi_n) \qquad (A.32)$$

with

$$\Phi_n = \tan^{-1}\left[\frac{Im(\mathbb{R}_n)}{Re(\mathbb{R}_n)}\right]$$

where

$$\mathbb{R}_n = R_{M+n} \qquad (A.33)$$

and

$$\mathbb{W}_n = W_{M+n} \qquad (A.34)$$

The baseband transmitted pulse train may be represented by equation (A.13) as

$$g_{trans}(t) = \sum_{n=0}^{k} \mathbb{W}_n \cos\, n\omega_o t \qquad (A.35)$$

Equation (A.32) will be a distorted and delayed version of equation (A.35). The comparison of the delay between the two equations represents the distance measurement. The left side of equation (A.32) can either be obtained by the indicated summation for any t or by using the inverse discrete Fourier transform on the complex amplitudes $\mathbb{W}_n\mathbb{R}_n$. The direct evaluation of equations (A.32) and (A.35) can produce the values of $f_{RWB}(t)$ for any value of t, so that a smooth curve can be obtained. The discrete Fourier transform also tends toward a smooth curve if the number of points is increased in the transform by adding zeroes for higher frequencies. The zero padded transform does an interpolation between points that is just what the Fourier series of equation (A.32) produces directly.

REFERENCES

1. Davies, K.: Ionospheric Radio Propagation. Dover Publications, Inc., New York, 1966.

2. Ginzburg, V.L.: The Propagation of Electromagnetic Waves in Plasmas. Pergamon Press, New York, 1970.

3. Picquenard, A.: Radio Wave Propagation. Halsted Press, New York, 1974.

4. Kelso, J.M.: Radio Propagation in the Ionosphere. McGraw-Hill Co.,Inc., New York, 1964.

5. Davies, K.: Ionospheric Radio Waves. Blaisdell Publishing Co., Waltham, Massachusetts, 1969.

6. Appleton, E.V.: URSI Proceedings. Washington, 1927.

7. Wait, J.R.: Electromagnetic Wave Theory. Harper and Row, New York, 1985.

8. Ichimaru, S.: Basic Principles of Plasma Physics. W.A. Benjamin, Inc., Reading, Massachusetts, 1973.

9. Kraus, J.D.: Electromagnetics, McGraw-Hill Book Co., New York, 1984.

10. Abramowitz, M. and Stegun, I.A.: Handbook of Mathematical Functions. National Bureau of Standards, U.S. Government Printing Office, Washington, D.C., May 1968.

11. Bracewell, R.: The Fourier Transform and Its Applications. McGraw-Hill, Inc., New York, 1965.

12. Shebalin, J.V.: Aerobrake Plasmadynamics: Macroscopic Effects. AIAA 90-1559, June 1990.

13. Gnoffo, P.: Conservation Equations and Physical Model for Hypersonic Air Flows in Thermal and Chemical Non-equilibrium. NASA TP-2867, February 1989.

TABLE I

REFLECTION COEFFICIENTS AT FRONT INTERFACE OF INHOMOGENEOUS LAYER-LINEAR PROFILE

	Runge-Kutta		Exact-Airy	
Frequency (GHz)	Real	Imag	Real	Imag
74.0000	1.0000	0.0000	1.0000	0.0000
74.0317	0.9682	0.2503	0.9682	0.2503
74.0635	0.8746	0.4848	0.8746	0.4848
74.0952	0.7252	0.6885	0.7252	0.6885
74.1270	0.5294	0.8484	0.5294	0.8484
74.1587	0.2996	0.9541	0.2996	0.9541
74.1905	0.0504	0.9987	0.0504	0.9987
74.2222	-0.2023	0.9793	-0.2023	0.9793
74.2540	-0.4422	0.8969	-0.4422	0.8969
74.2857	-0.6538	0.7566	-0.6539	0.7566
74.3175	-0.8235	0.5673	-0.8236	0.5672
74.3492	-0.9401	0.3410	-0.9401	0.3408
74.3810	-0.9957	0.9222	-0.9958	0.9207
74.4127	-0.9867	-0.1628	-0.9866	-0.1630
74.4444	-0.9132	-0.4076	-0.9131	-0.4078
74.4762	-0.7799	-0.6259	-0.7797	-0.6261
74.5079	-0.5953	-0.8035	-0.5951	-0.8036
74.5397	-0.3715	-0.9285	-0.3712	-0.9286
74.5714	-0.1229	-0.9924	-0.1227	-0.9924
74.6032	0.1339	-0.9910	0.1341	-0.9910
74.6349	0.3820	-0.9242	0.3822	-0.9241
74.6667	0.6050	-0.7962	0.6052	-0.7960
74.6984	0.7881	-0.6155	0.7883	-0.6153
74.7302	0.9191	-0.3939	0.9192	-0.3937
74.7619	0.9893	-0.1462	0.9893	-0.1460
74.7937	0.9938	0.1114	0.9938	0.1116
74.8254	0.9323	0.3617	0.9322	0.3619

TABLE I (continued)

Frequency (GHz)	Runge-Kutta		Exact-Airy	
	Real	Imag	Real	Imag
74.8571	0.8088	0.5881	0.8087	0.5882
74.8889	0.6314	0.7754	0.6313	0.7755
74.9206	0.4119	0.9112	0.4118	0.9113
74.9524	0.1647	0.9864	0.1645	0.9864
74.9841	-0.9377	0.9956	-0.9390	0.9956
75.0159	-0.3462	0.9382	-0.3463	0.9381

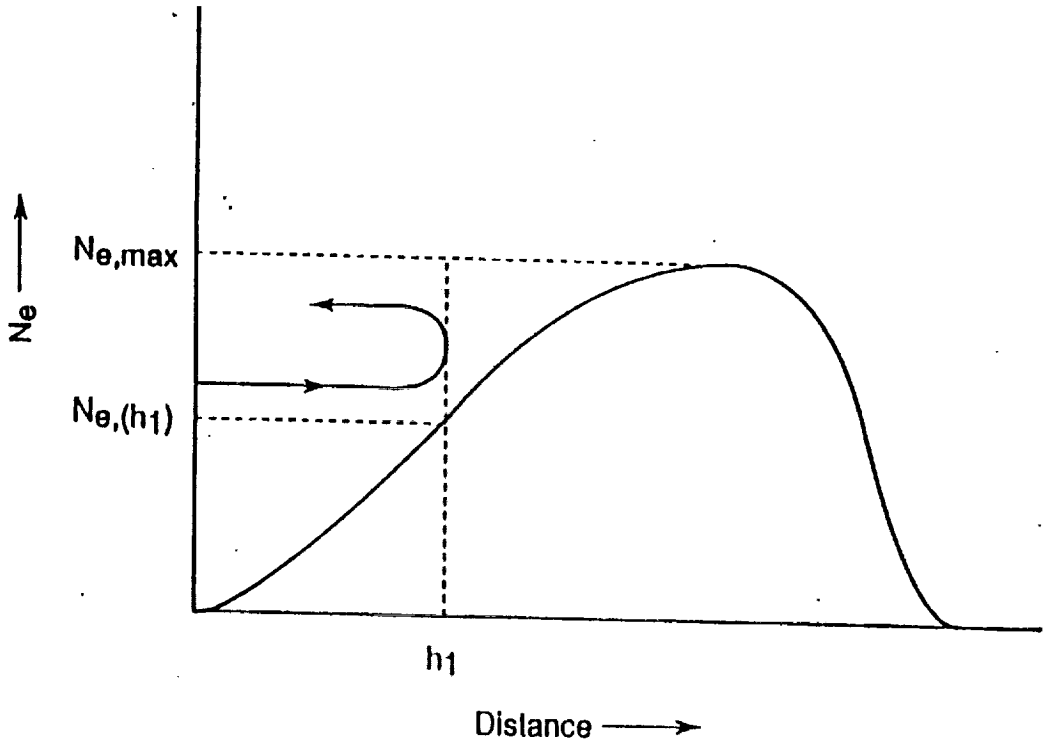

Figure 1 Reflection from a sample plasma electron density profile as a function of distance. The turning point is located at h_1.

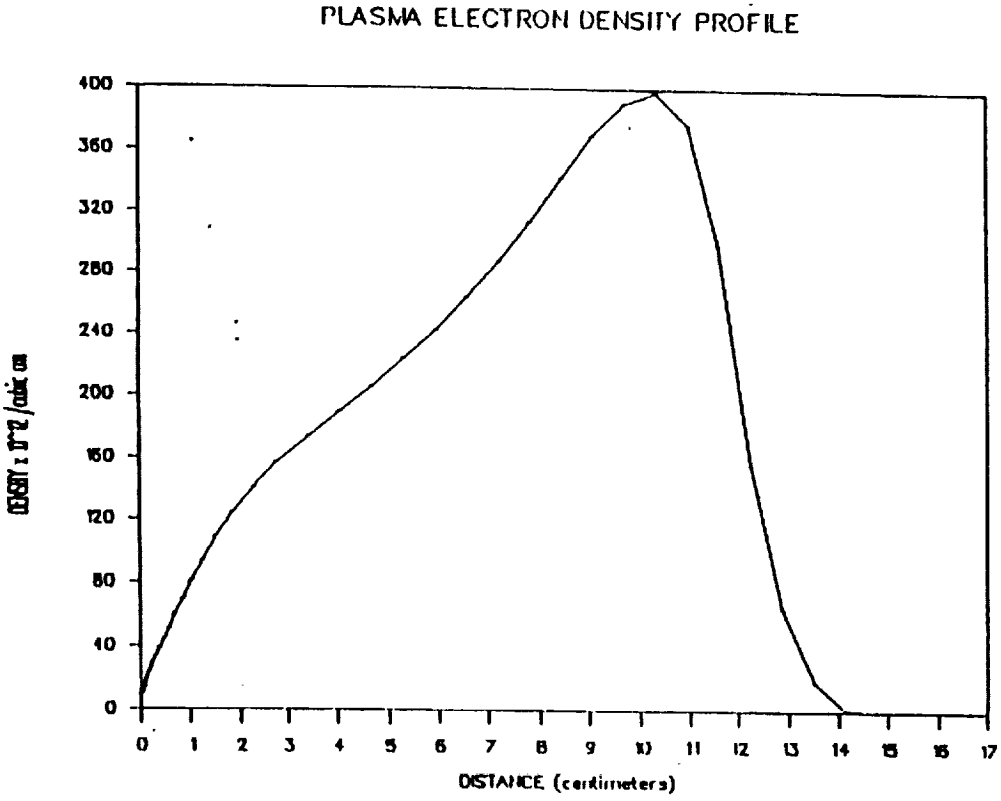

Figure 2 Electron density profile prediction for MRIS. [P. Gnoffo, "Conservation Equations and Physical Model for Hypersonic Air Flows in Thermal and Chemical Non-equilibrium." NASA TP-2867, February 1989.]

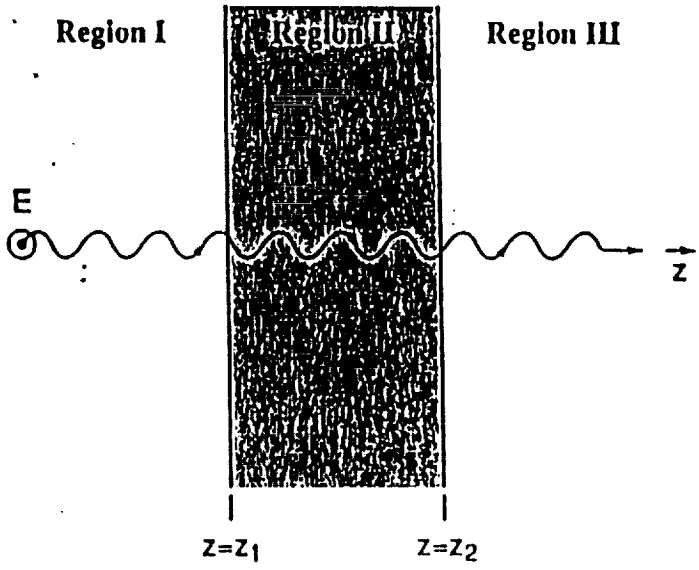

Figure 3 Plane wave incident on a plane uniform dielectric (Region II). Regions I and III are free space.

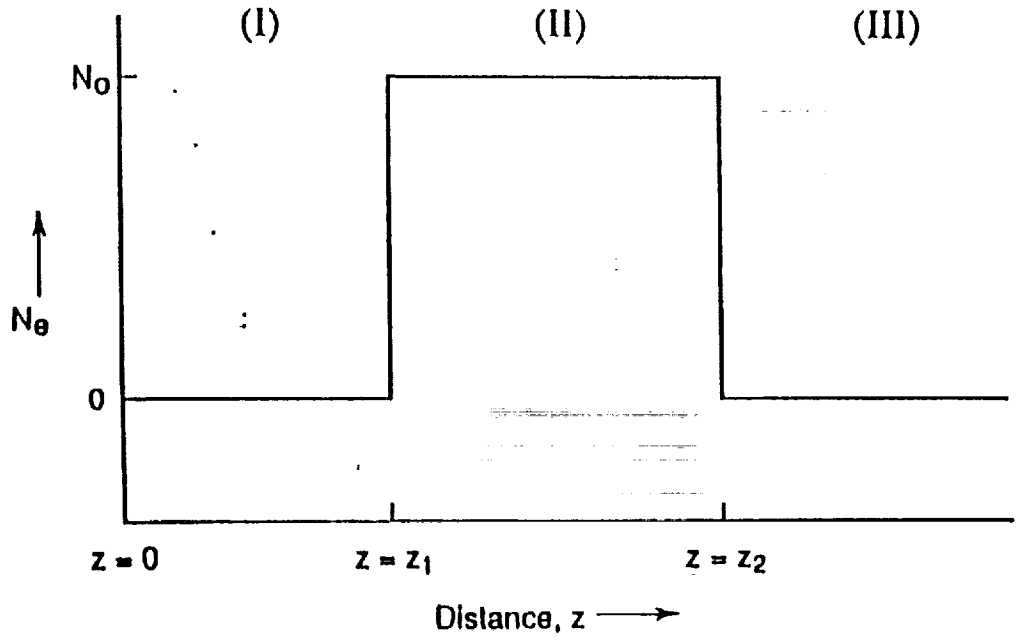

Figure 4 Electron density profile for a uniform dielectric (Region II) between free space regions I and III.

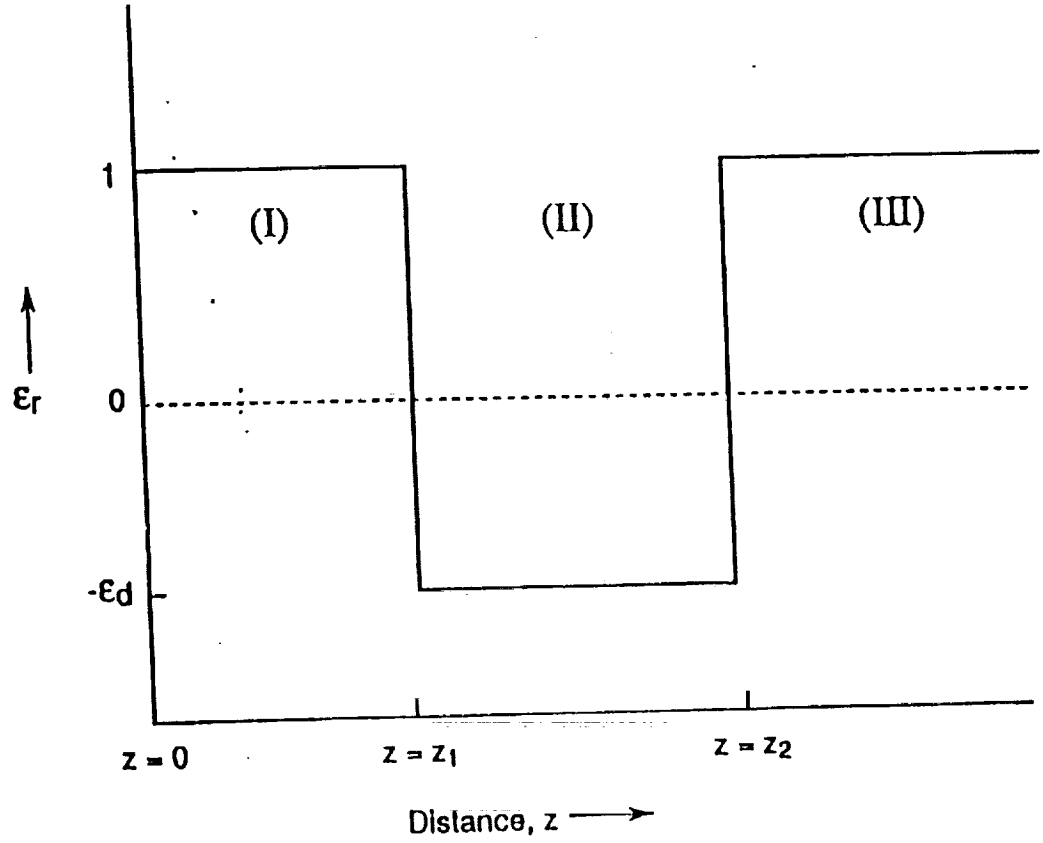

Figure 5 Relative permittivity of a uniform dielectric (Region II) between free space regions I and III.

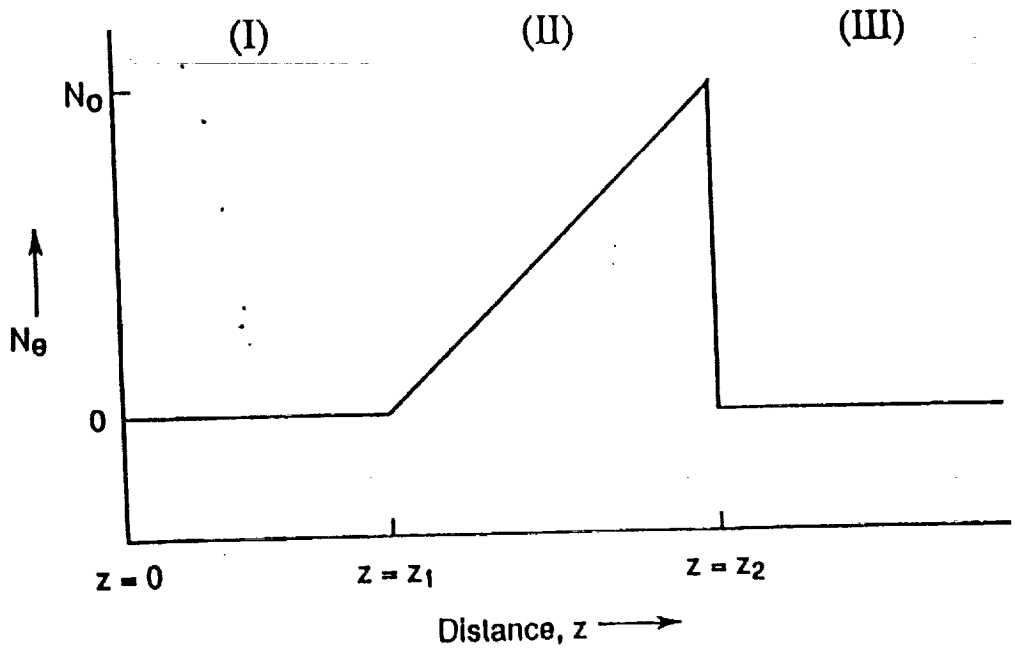

Figure 6 Electron density profile for a linear layer (Region II) between free space regions I and III.

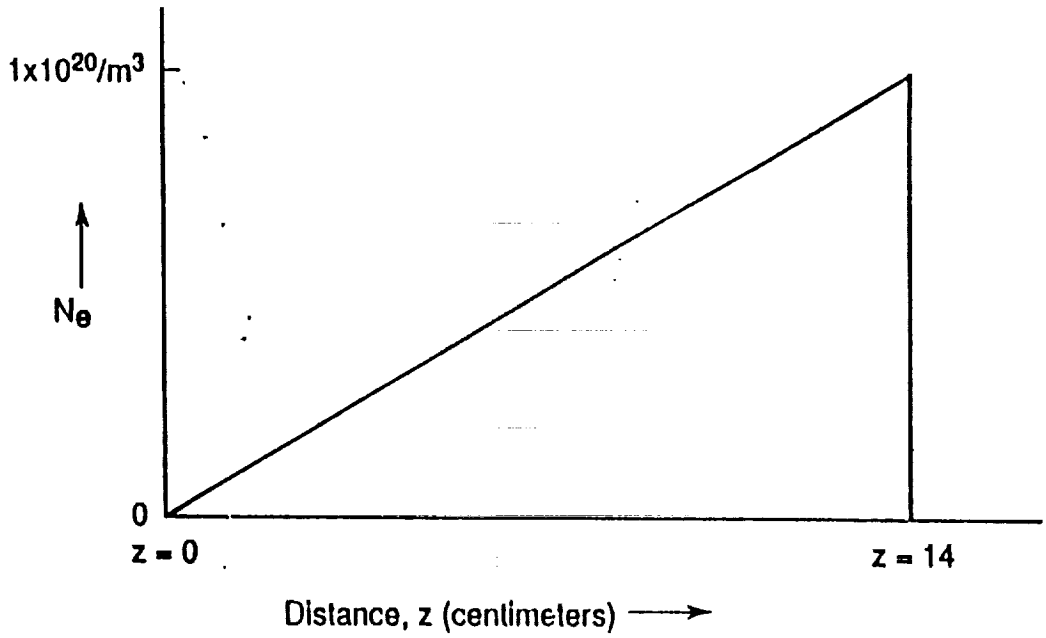

Figure 7 Sample linear electron density profile.

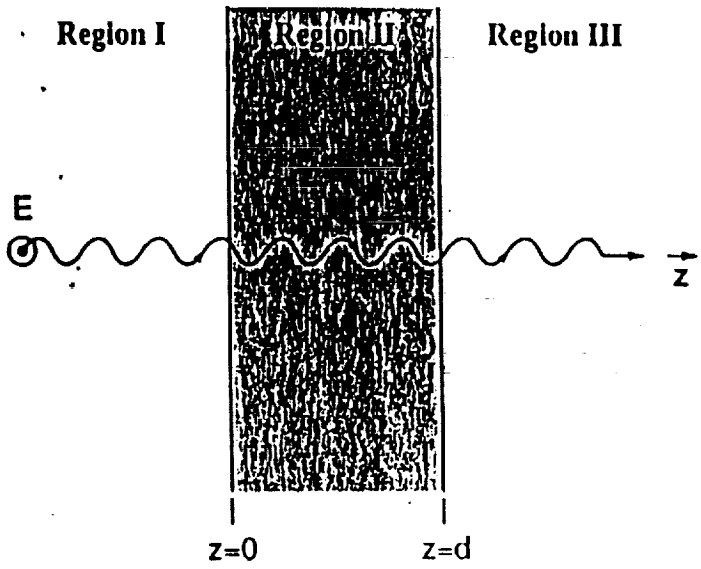

Figure 8 Plane wave incident on a plasma layer (Region II) surrounded by free space (Regions I and III).

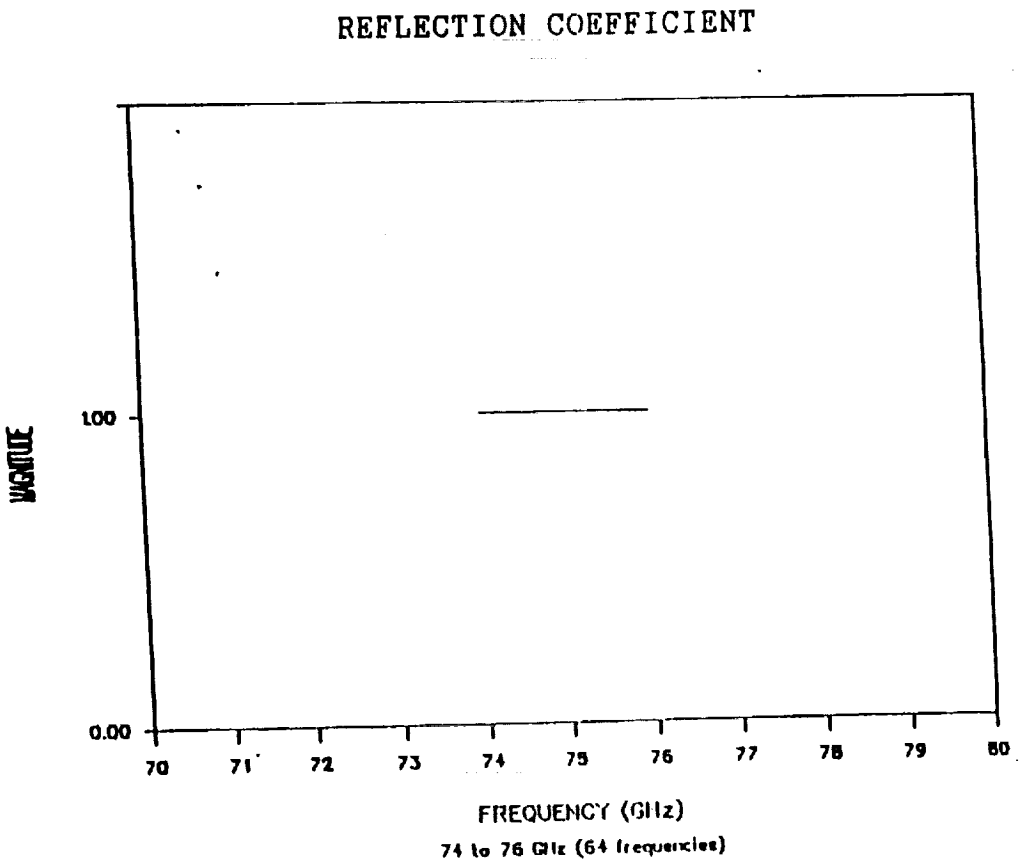

Figure 9 Magnitude of the reflection coefficient for a 14 cm. thick uniform dielectric slab (ϵ_r=-0.5) located 10 cm. from measurement plane.

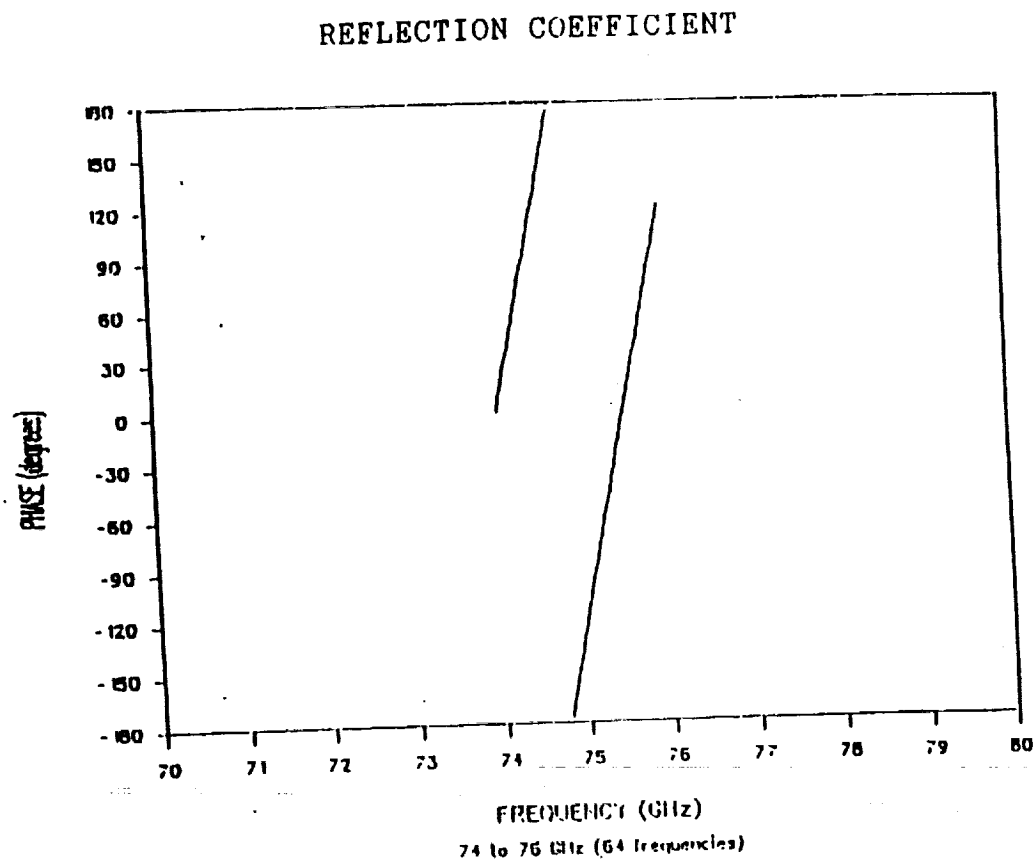

Figure 10 Phase of the reflection coefficient for a 14 cm. thick uniform dielectric slab (ϵ_r=-0.5) located 10 cm. from measurement plane.

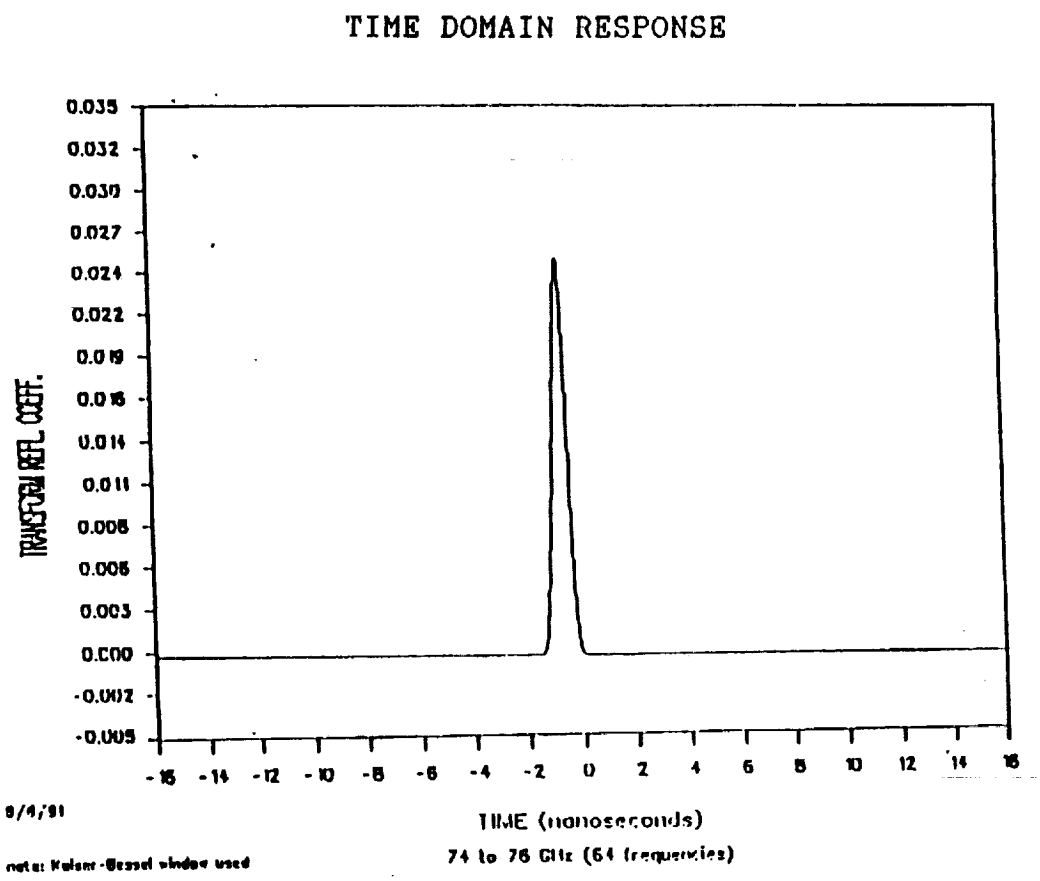

Figure 11 Time domain response for a 14 cm. thick uniform dielectric slab (ε_r=-0.5) located 10 cm. from measurement plane.

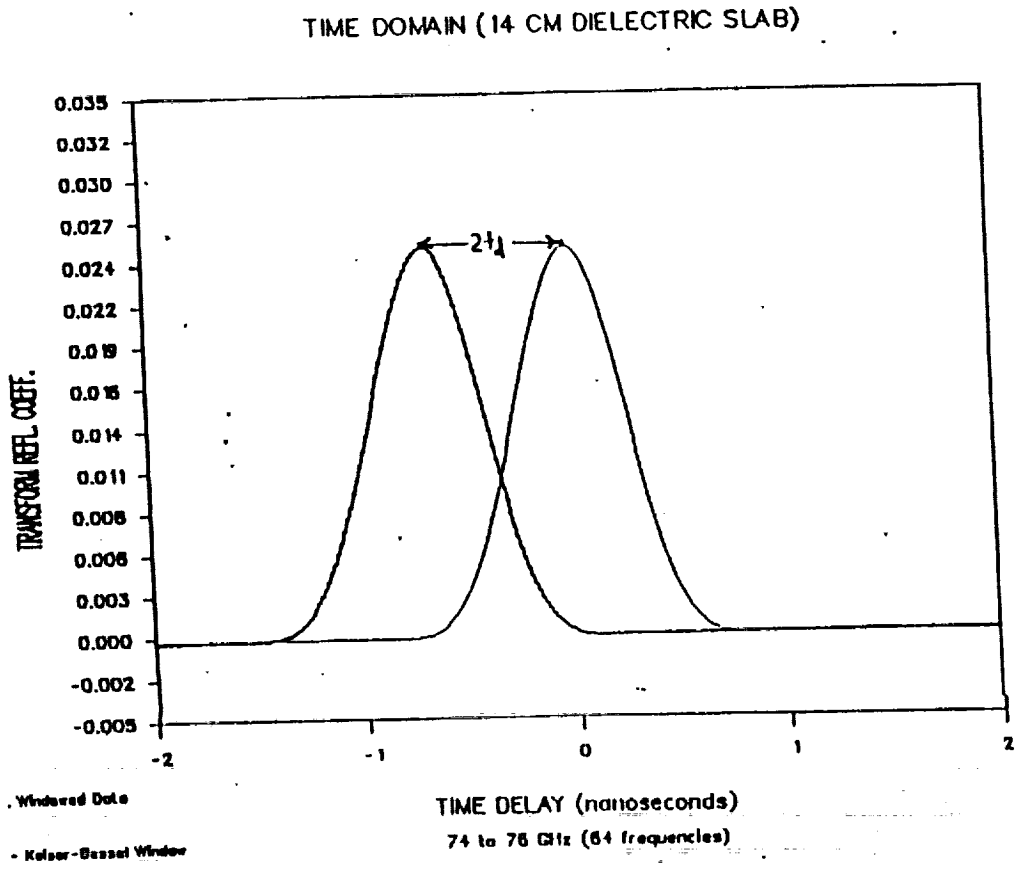

Figure 12 Propagation delay for a 14 cm. thick uniform dielectric slab (ϵ_r=-0.5). The shift $2t_d$ corresponds to the round-trip propagation delay. The delay is measured on the negative side of the time axis.

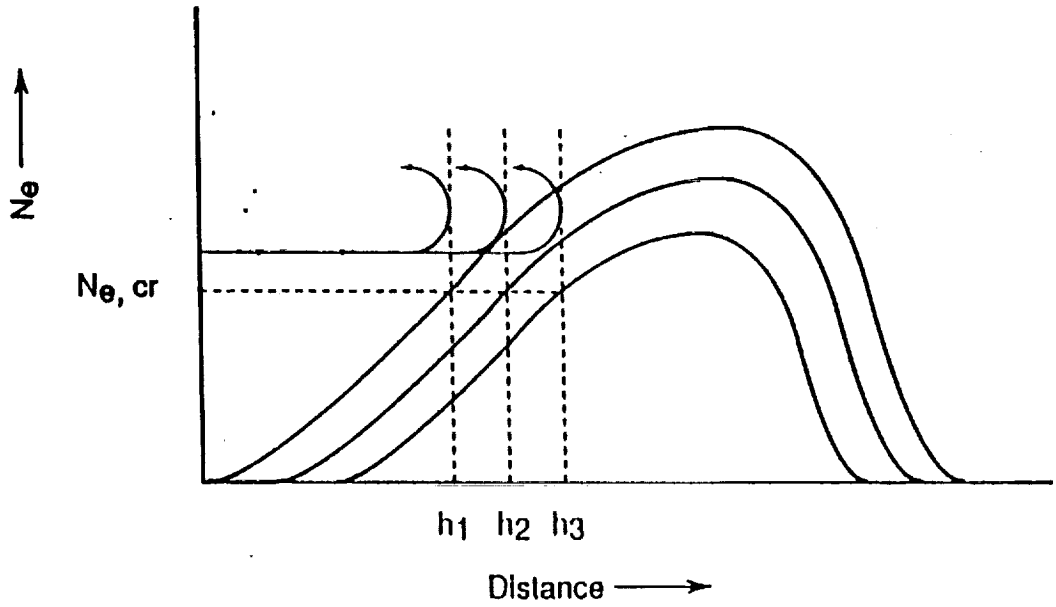

Figure 13 Reduction of sample electron density profile where the critical electron density level is $N_{e,cr}$. The turning point moves from h_1 to h_2 and then h_3 as the profile is reduced.

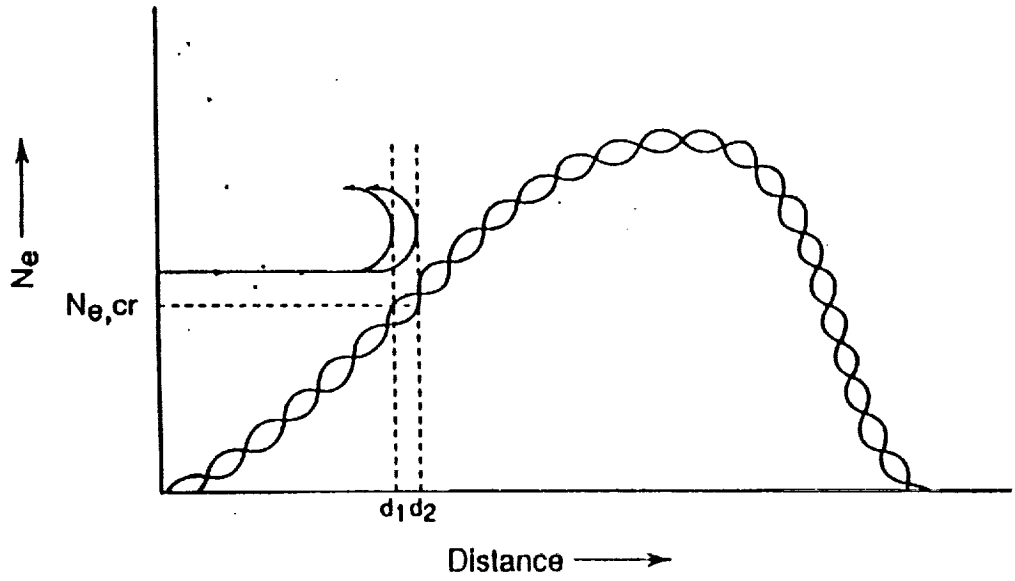

Figure 14 Modulation of sample electron density profile where the critical electron density level is $N_{e,cr}$. The turning point moves from d_1 to d_2 as the ripple on the profile changes.

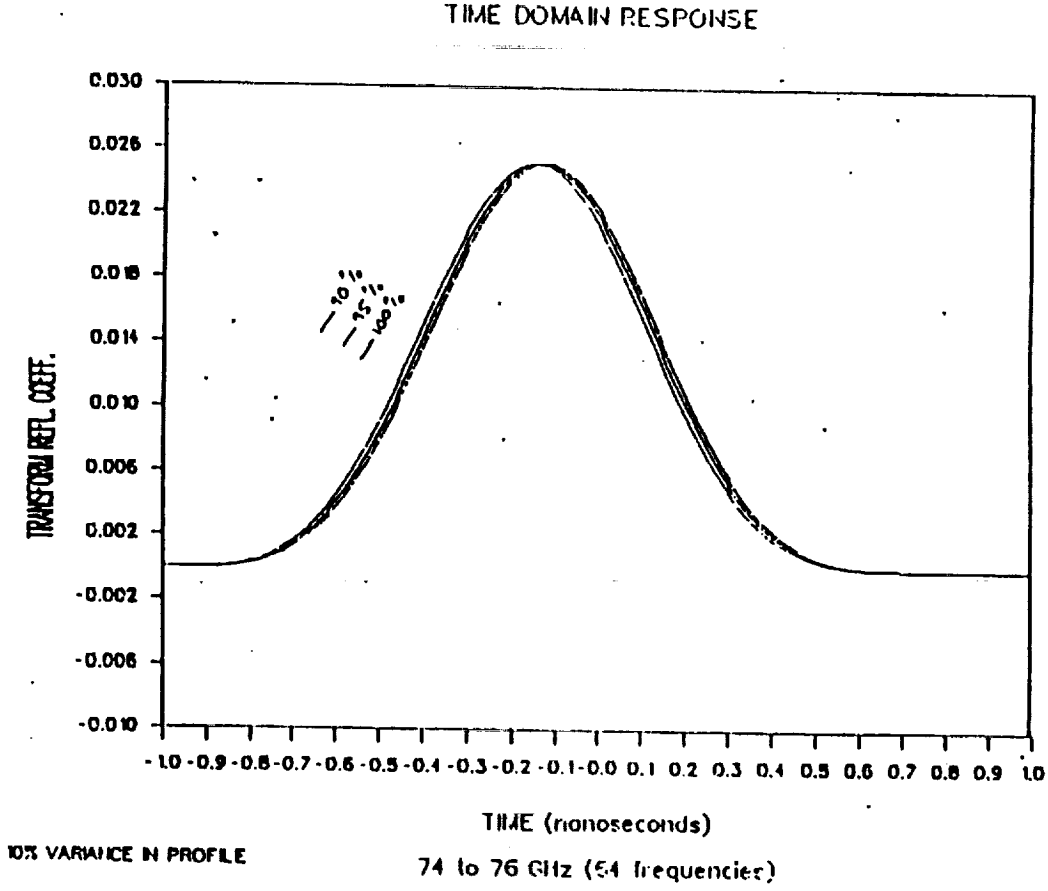

Figure 15 Time domain responses for reduced electron density profiles for 74 to 76 GHz. Shown are responses for 100%, 95% and 90% values for the profile.

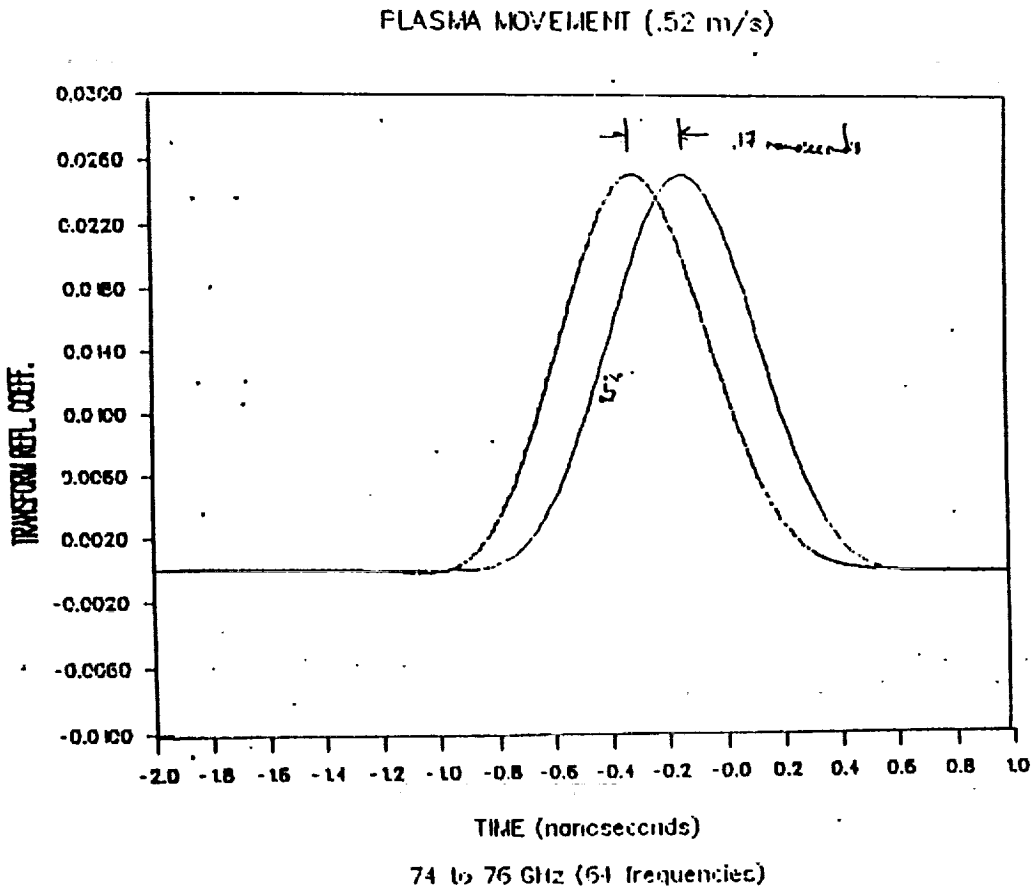

Figure 16 Time domain response for a 10% reduction in electron density profile. The 95% response is used as a reference.

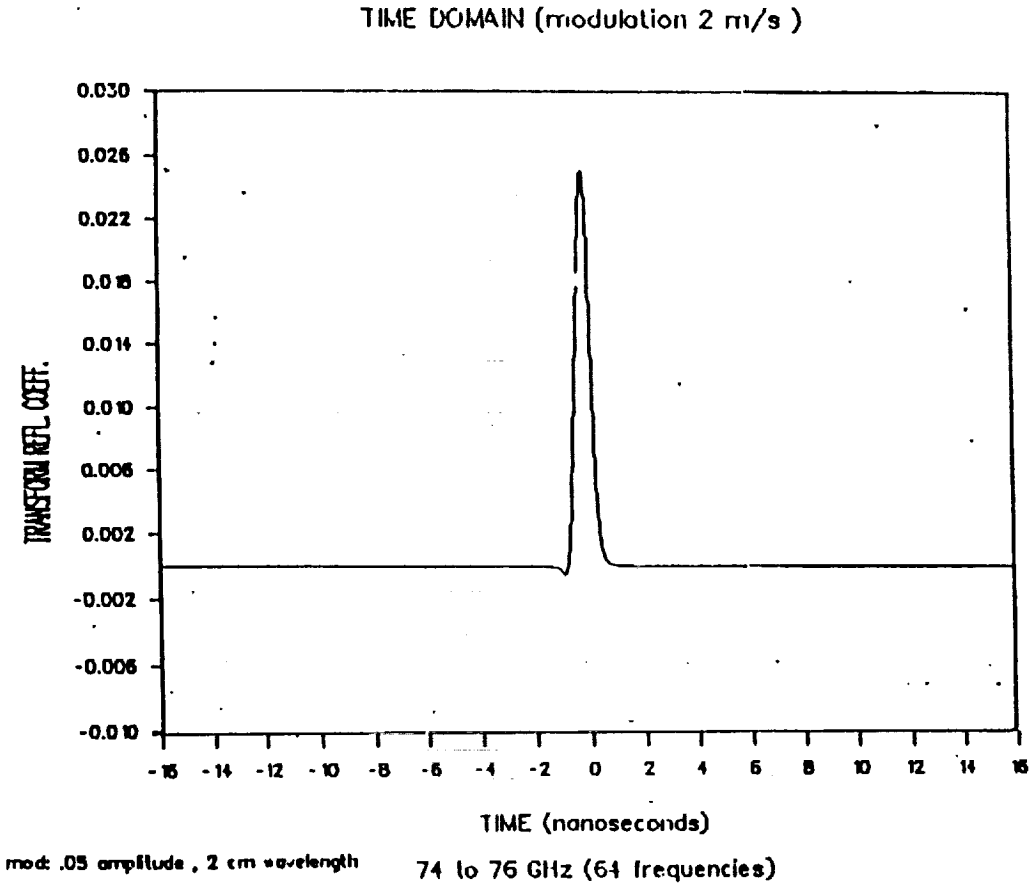

Figure 17 Transform reflection coefficient for a modulated electron density profile for 74 to 76 GHz with modulation amplitude, A=.05 and modulation velocity at 2 m/s.

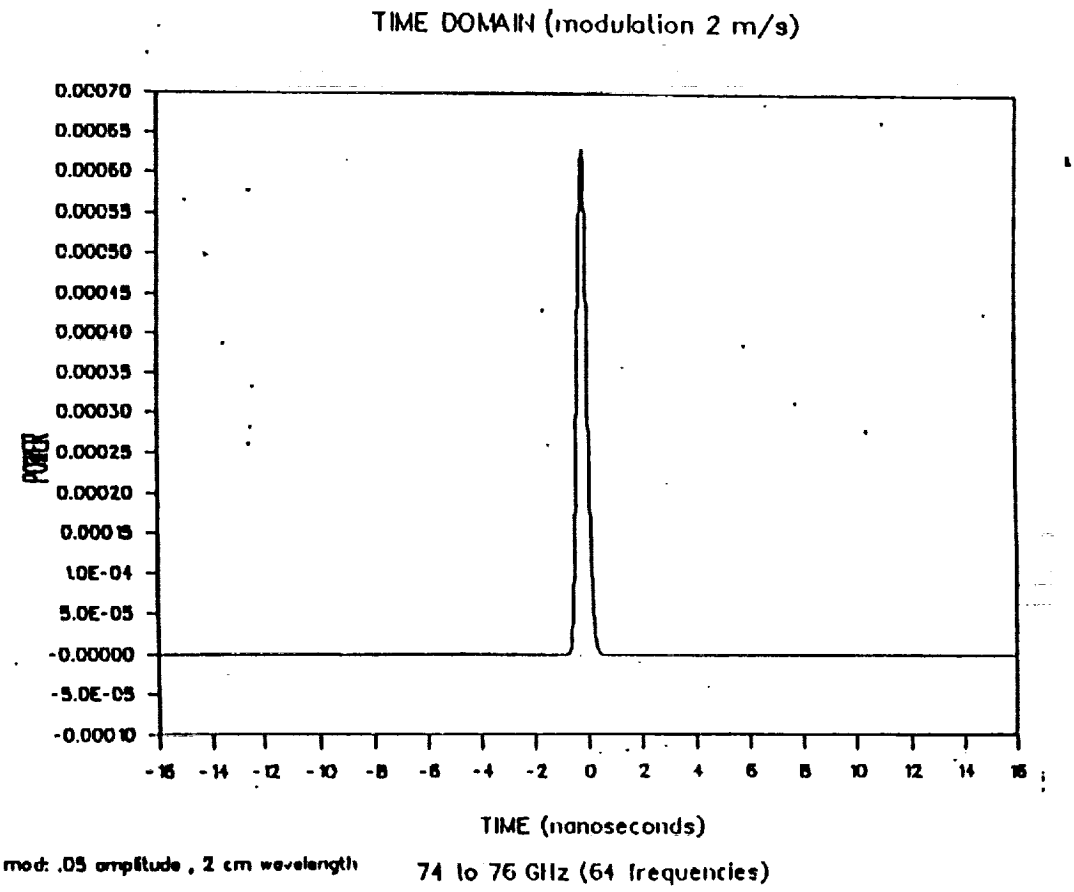

Figure 18 Time domain response (Power) for a modulated electron density profile for 74 to 76 GHz with modulation amplitude, A=.05 and modulation velocity at 2 m/s.

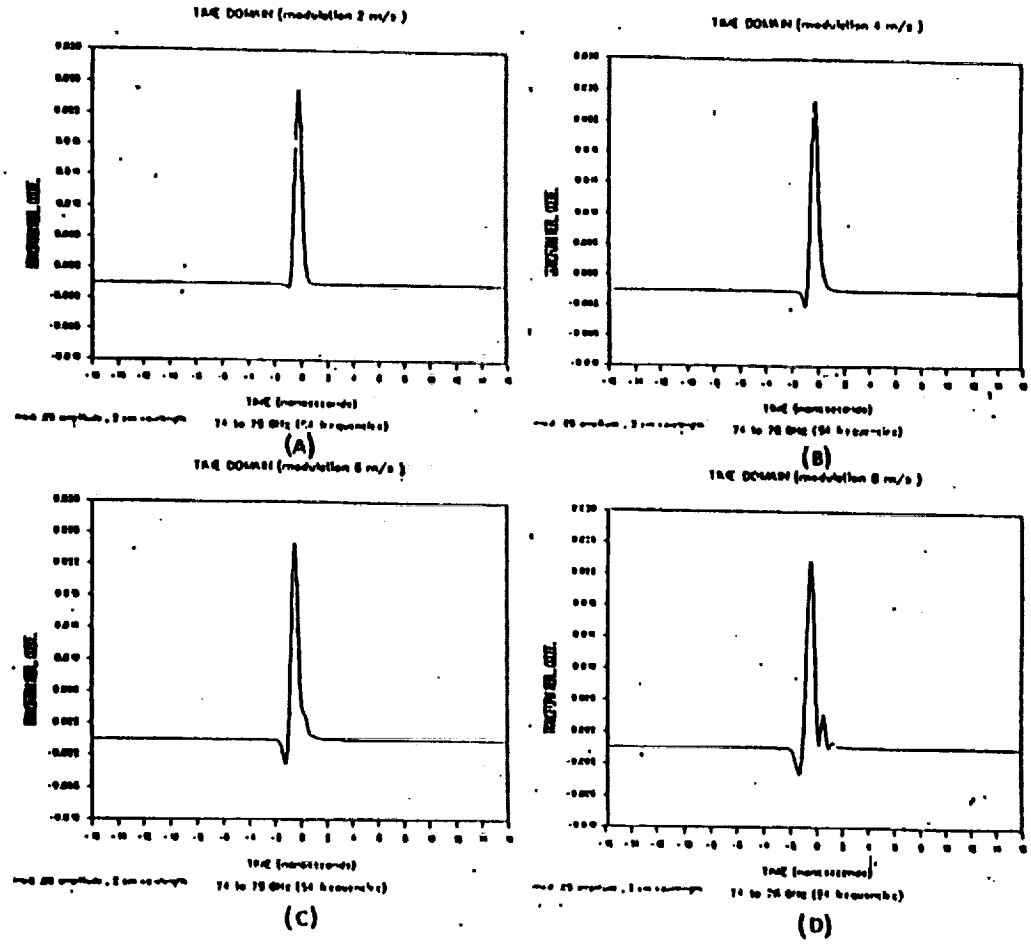

Figure 19 Transform reflection coefficient for 74 to 76 GHz with modulation amplitude, A=.05 and modulation velocity at (a) 2 m/s, (b) 4 m/s, (c) 6 m/s and (d) 8 m/s.

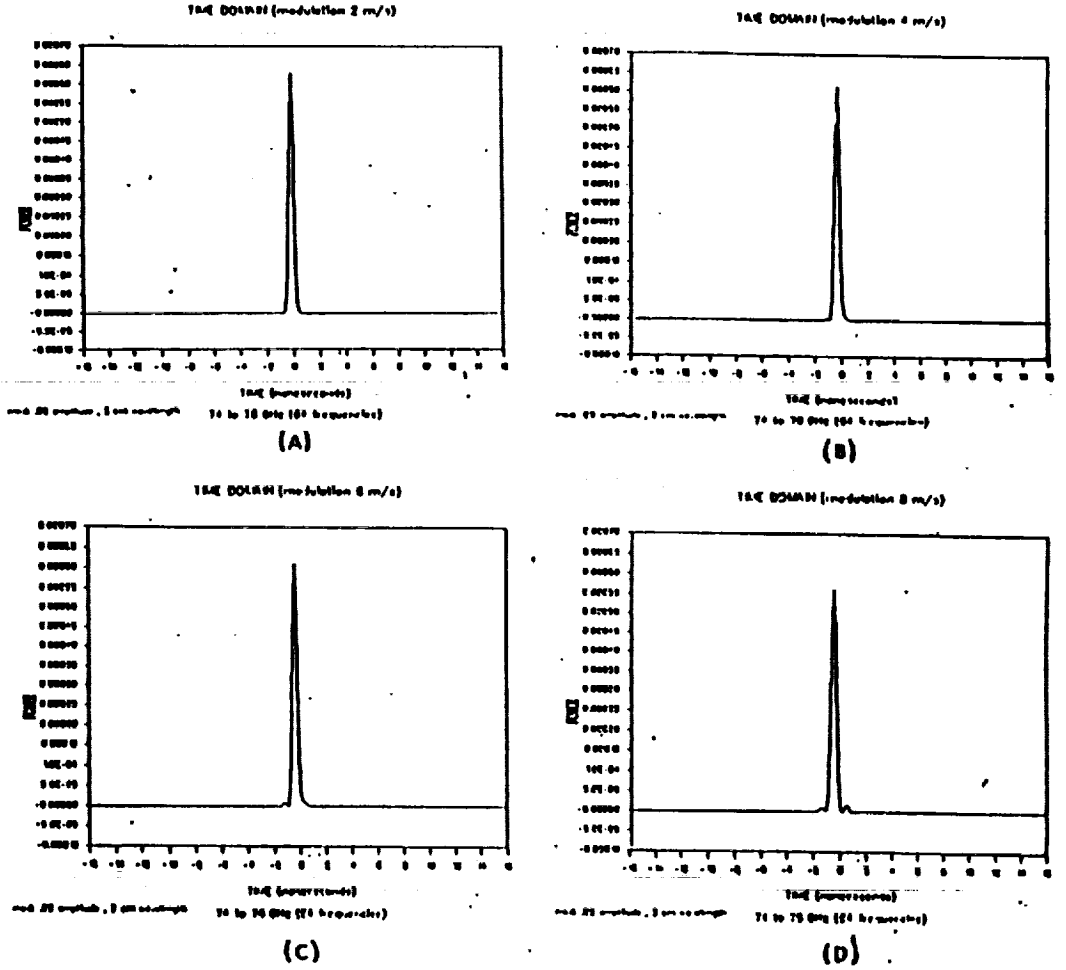

Figure 20 Time domain response (Power) for 74 to 76 GHz with modulation amplitude, A=.05 and modulation velocity at (a) 2 m/s, (b) 4 m/s, (c) 6 m/s and (d) 8 m/s.

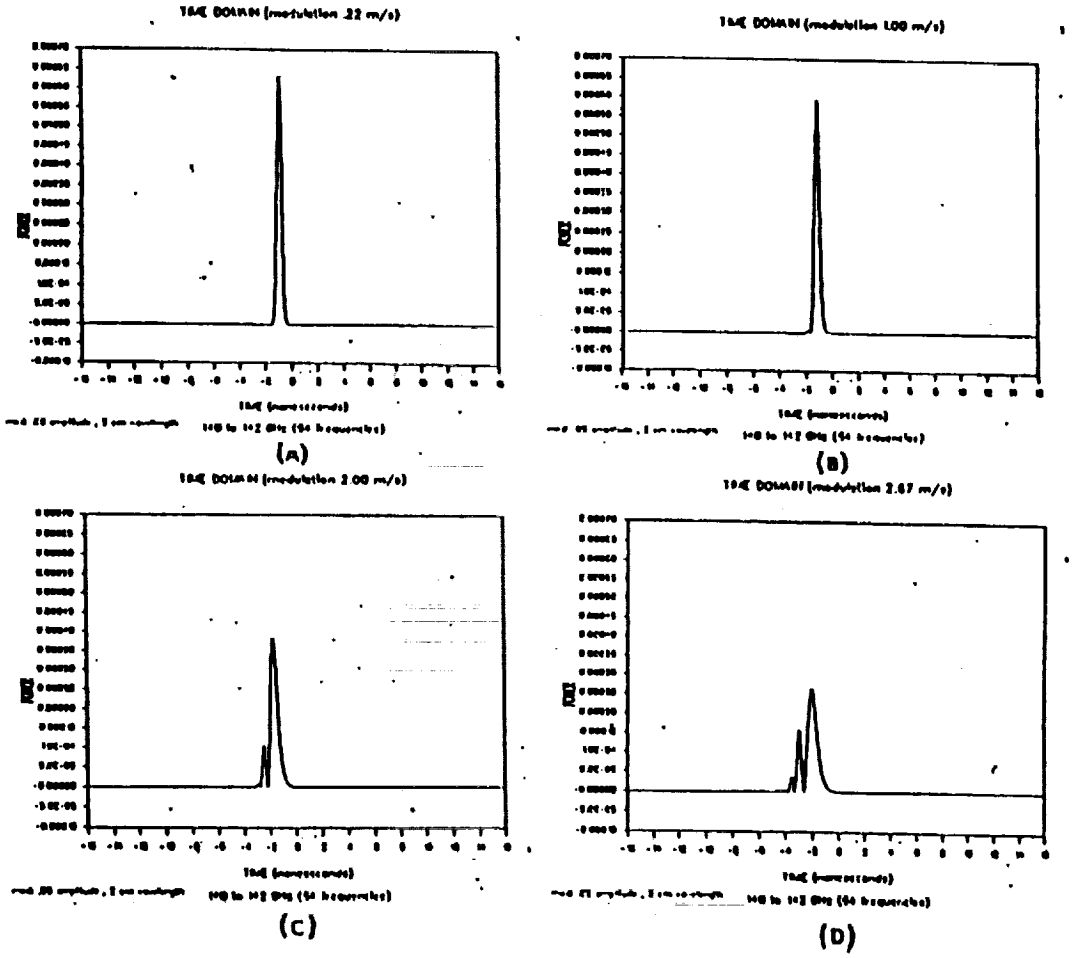

Figure 21 Time domain response for 140 to 142 GHz with modulation amplitude, A=.05 and modulation velocity at (a) .22 m/s, (b) 1.00 m/s, (c) 2.00 m/s and (d) 2.67 m/s.

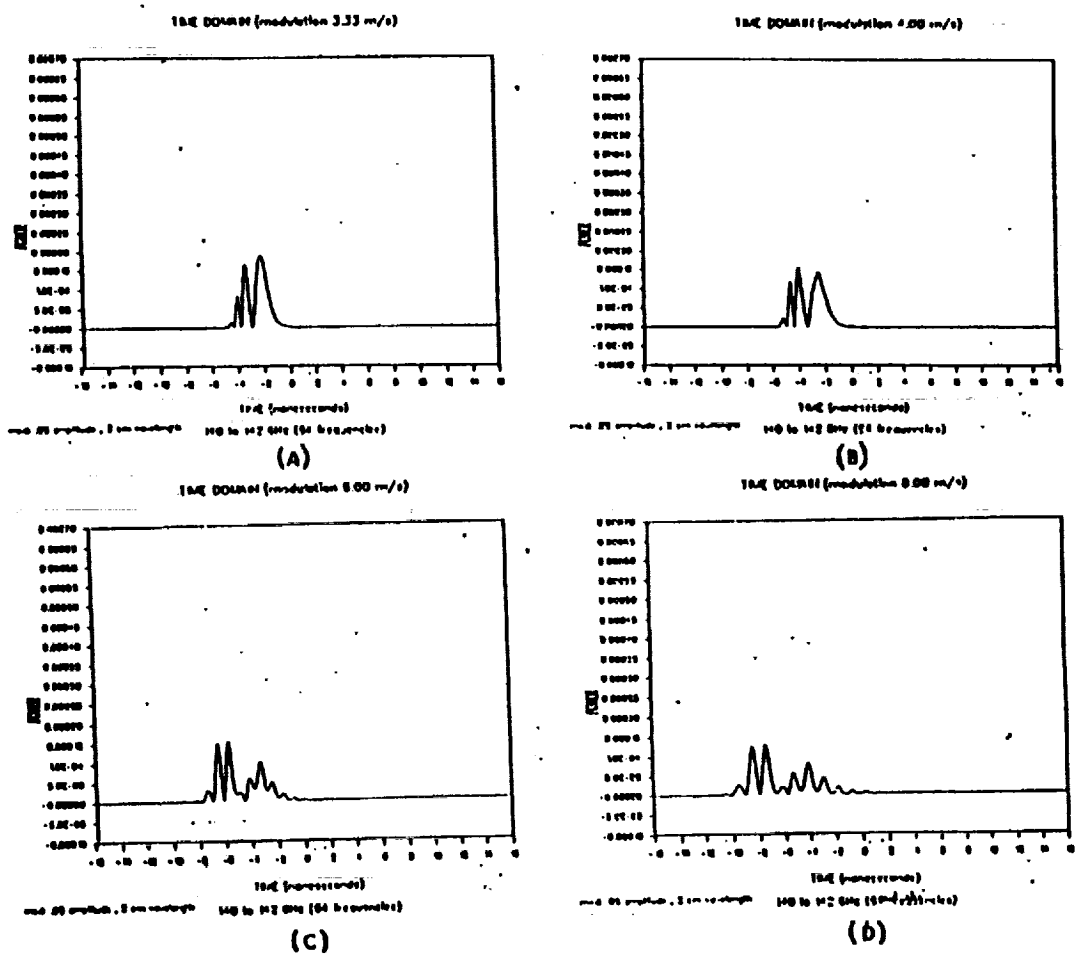

Figure 22 Time domain response for 140 to 142 GHz with modulation amplitude, A=.05 and modulation velocity at. (a) 3.33 m/s, (b) 4.00 m/s, (c) 6.00 m/s and (d) 8.00 m/s.

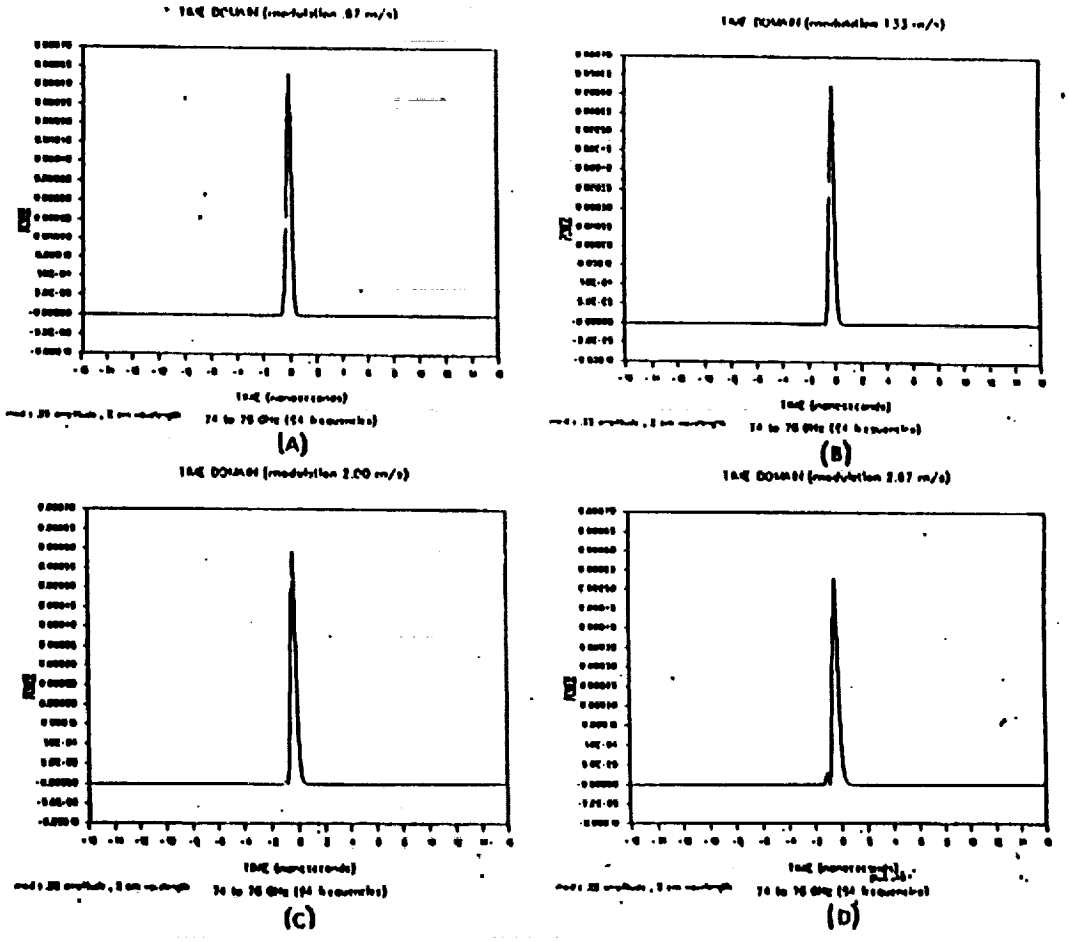

Figure 23 Time domain response for 74 to 76 GHz with modulation amplitude, A=.25 and modulation velocity at (a) .67 m/s, (b) 1.33 m/s, (c) 2.00 m/s and (d) 2.67 m/s.

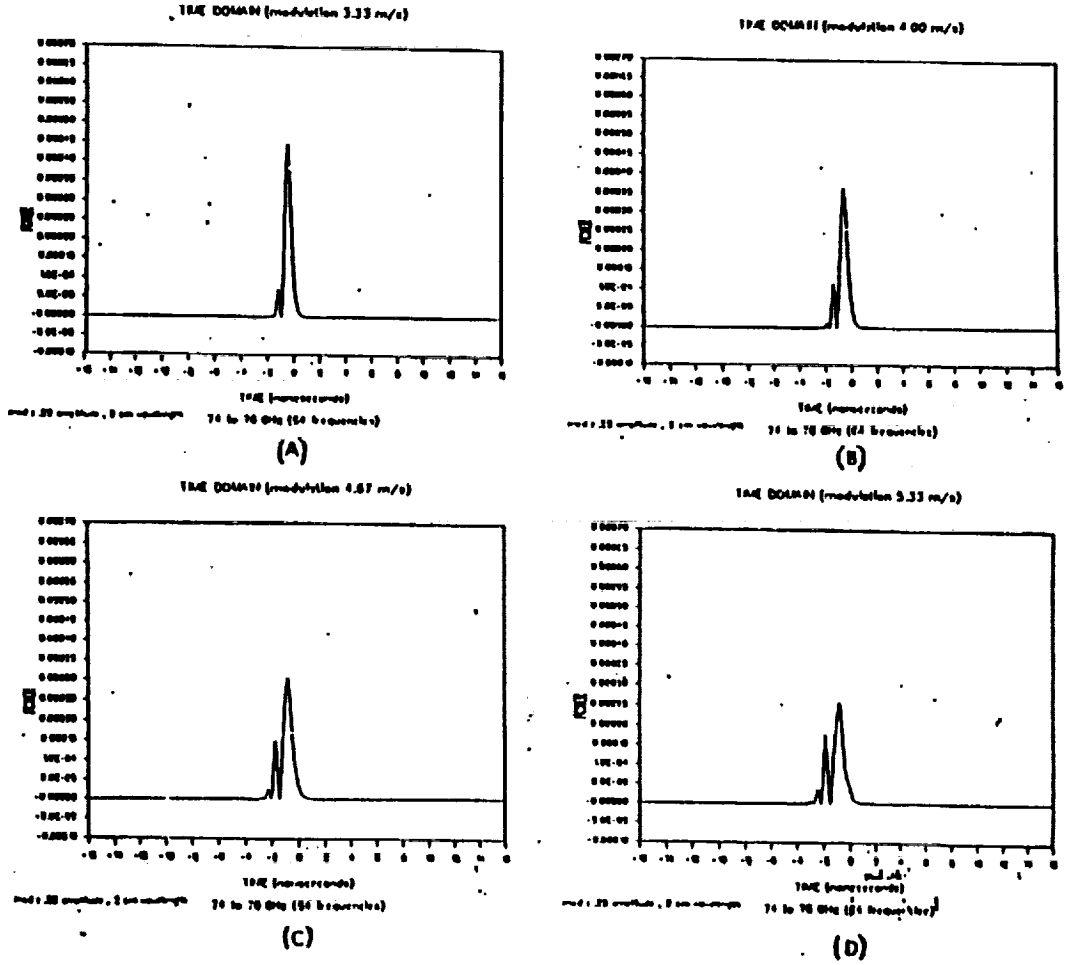

Figure 24 Time domain response for 74 to 76 GHz with modulation amplitude, A=.25 and modulation velocity at (a) 3.33 m/s, (b) 4.00 m/s, (c) 4.67 m/s and (d) 5.33 m/s.

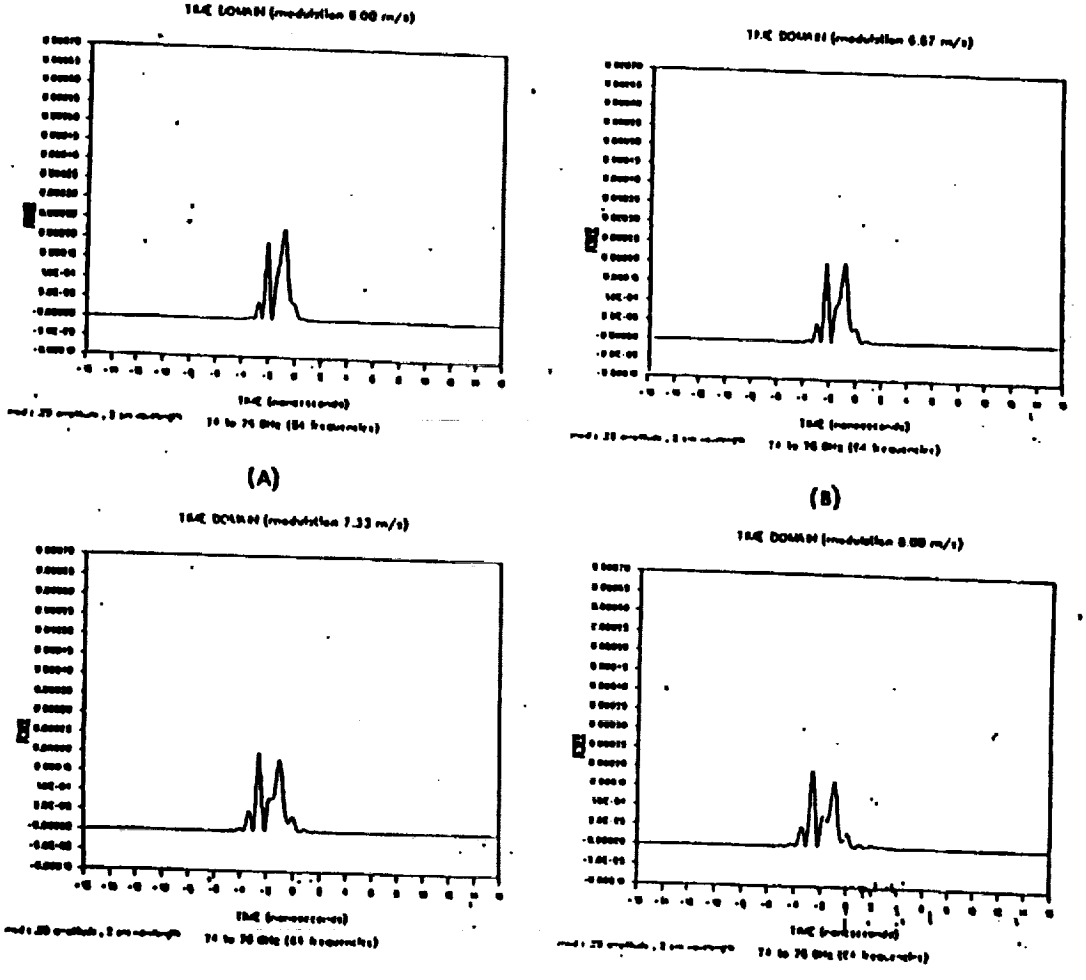

Figure 25 Time domain response for 74 to 76 GHz with modulation amplitude, A=.25 and modulation velocity at (a) 6.00 m/s, (b) 6.67 m/s, (c) 7.33 m/s and (d) 8.00 m/s.

REPORT DOCUMENTATION PAGE

Form Approved
OMB No. 0704-0188

1. AGENCY USE ONLY *(Leave blank)*	2. REPORT DATE	3. REPORT TYPE AND DATES COVERED
	September 1992	Technical Memorandum

4. TITLE AND SUBTITLE
Time Domain Reflectometry in Time Variant Plasmas

5. FUNDING NUMBERS
WU 505-64-70-01

6. AUTHOR(S)
Michael J. Scherner

7. PERFORMING ORGANIZATION NAME(S) AND ADDRESS(ES)
NASA Langley Research Center
Hampton, VA 23665-5225

8. PERFORMING ORGANIZATION REPORT NUMBER

9. SPONSORING/MONITORING AGENCY NAME(S) AND ADDRESS(ES)
National Aeronautics and Space Administration
Washington, DC 20546-0001

10. SPONSORING/MONITORING AGENCY REPORT NUMBER
NASA TM-104056

11. SUPPLEMENTARY NOTES

12a. DISTRIBUTION/AVAILABILITY STATEMENT
unclassified - unlimited

subject category 75

12b. DISTRIBUTION CODE

13. ABSTRACT *(Maximum 200 words)*

The effects of time-dependent electron density fluctuations on a synthesized time domain reflectometry response of a one-dimensional cold plasma sheath are considered. Numerical solutions of the Helmholtz wave equation, which describes the electric field of a normally incident plane wave in a specified static electron density profile, are used. Included in this work is a study of the effects of Doppler shifts resulting from moving density fluctuations in the electron density profile of the sheath. Varying electron density levels corrupt time domain and distance measurements. Reducing or modulating the electron density levels of a given electron density profile affects the time domain response of a plasma and results in motion of the turning point, and the effective motion has a significant effect on measuring electron density locations.

14. SUBJECT TERMS	15. NUMBER OF PAGES
time-dependent, electron, density, Doppler, fluctuations	79
	16. PRICE CODE: A05

17. SECURITY CLASSIFICATION OF REPORT	18. SECURITY CLASSIFICATION OF THIS PAGE	19. SECURITY CLASSIFICATION OF ABSTRACT	20. LIMITATION OF ABSTRACT
unclassified	unclassified	unclassified	